

Mouse T cell priming is enhanced by maturation-dependent stiffening of the dendritic cell cortex

Daniel Blumenthal, Vidhi Chandra, Lyndsay Avery, and Janis K. Burkhardt*

Department of Pathology and Laboratory Medicine,
Children's Hospital of Philadelphia Research Institute and
Perelman School of Medicine at the University of Pennsylvania,
Philadelphia, PA, USA

***Correspondence:**

Janis K. Burkhardt
Department of Pathology and Laboratory Medicine
Children's Hospital of Philadelphia Research Institute
3615 Civic Center Blvd, ARC 816D,
Philadelphia, PA 19104, USA
Tel: 267-426-5410
E-mail: jburkhar@pennmedicine.upenn.edu

Running Title: Modulation of T cell activation by dendritic cell cortical stiffness

Key Words: actin, mechanotransduction, maturation, costimulation, signaling, cytoskeleton

1 **ABSTRACT**

2 T cell activation by dendritic cells (DCs) involves forces exerted by the T cell actin cytoskeleton,
3 which are opposed by the cortical cytoskeleton of the interacting APC. During an immune
4 response, DCs undergo a maturation process that optimizes their ability to efficiently prime
5 naïve T cells. Using atomic force microscopy, we find that **during maturation**, DC cortical
6 stiffness increases via a process that involves actin polymerization. Using stimulatory hydrogels
7 and DCs expressing mutant cytoskeletal proteins, we find that **increasing stiffness lowers the**
8 **agonist dose needed for T cell activation.** CD4⁺ T cells exhibit much more profound stiffness-
9 dependency than CD8⁺ T cells. Finally, stiffness responses are most robust when T cells are
10 stimulated **with pMHC** rather than anti-CD3ε, consistent with a mechanosensing mechanism
11 involving **receptor deformation**. Taken together, our data reveal that maturation-associated
12 cytoskeletal changes alter the biophysical properties of DCs, providing mechanical cues that
13 costimulate T cell activation.

14 INTRODUCTION

15 The initiation of an adaptive immune response requires priming of naïve T cells by professional
16 antigen presenting cells (APCs). This process involves multiple receptor-ligand interactions,
17 which occur in concert at a specialized cell-cell contact site called the immunological synapse
18 (Dustin, 2014). Through these interactions, APCs transmit a highly orchestrated series of signals
19 that induce T cell activation and direct differentiation of T cell populations (Friedl, den Boer, &
20 Gunzer, 2005). While the biochemical aspects of this process have been the subject of many
21 studies, the contribution of mechanical cues is only now being uncovered.

22 Following initial T cell receptor (TCR) engagement, **T cells apply pushing and pulling forces on**
23 **interacting APCs** (Bashour et al., 2014; Blumenthal & Burkhardt, 2020; Hui, Balagopalan,
24 Samelson, & Upadhyaya, 2015; Husson, Chemin, Bohineust, Hivroz, & Henry, 2011; Sawicka et
25 al., 2017). **These forces are essential for proper T cell activation** (Li et al., 2010; Pryshchep,
26 Zarnitsyna, Hong, Evavold, & Zhu, 2014). Moreover, **force application** is responsible, at least in
27 part, for the **ability of T cells to rapidly discriminate between agonist and antagonist antigens**
28 (Das et al., 2015; Liu, Chen, Evavold, & Zhu, 2014). While the mechanism by which force is
29 translated into biochemical cues remains controversial (Das et al., 2015; Hong et al., 2015; Kim
30 et al., 2009), there is evidence that early tyrosine phosphorylation events downstream of TCR
31 engagement occur at sites where applied force is maximal (Bashour et al., 2014). Interestingly,
32 the amount of force a T cell applies is directly affected by the stiffness of the stimulatory
33 substrate (Husson et al., 2011; Sawicka et al., 2017). Thus, it appears that force application is
34 mechanically coupled to the T cell's ability to sense stiffness (mechanosensing). In other cell
35 types, substrate stiffness has been shown to affect a variety of cell functions including
36 differentiation, migration, growth and survival (Byfield, Reen, Shentu, Levitan, & Gooch, 2009;
37 Discher, Janmey, & Wang, 2005; Engler, Sen, Sweeney, & Discher; Lo, Wang, Dembo, & Wang;

38 Oakes et al., 2009; Pelham & Wang, 1997; Solon, Levental, Sengupta, Georges, & Janmey;
39 Trappmann et al., 2012). Stiffness sensing in T cells has not been well studied, though there is
40 some evidence that substrate stiffness affects both initial priming and effector functions
41 (Alatoom et al., 2020; Basu et al., 2016; Judokusumo, Tabdanov, Kumari, Dustin, & Kam, 2012;
42 O'Connor et al., 2012; Saitakis et al., 2017). Since the physiologically relevant substrate for T cell
43 priming is the surface of the interacting APC, one might predict that changes in cortical stiffness
44 of the APC will profoundly influence T cell priming. However, this prediction remains untested,
45 and studies addressing the role of substrate stiffness in T cell priming did not take into
46 consideration the physiological stiffness of APCs.

47 Dendritic cells (DCs) are the dominant APCs that prime T cells *in vivo* (Jung et al., 2002). One of
48 the hallmarks of DC biology is the process of maturation. Immature DCs are sentinels of the
49 immune system, specialized for immune surveillance and antigen processing (Mellman &
50 Steinman, 2001). In response to infection or injury, inflammatory stimuli trigger signaling
51 pathways that induce molecular reprogramming of the cell. The resulting mature DCs express
52 high levels of surface ligands and cytokines needed for efficient T cell priming (Burns et al.,
53 2004). A central feature of DC maturation is remodeling of the actin cytoskeleton, a process that
54 underlies other maturation-associated changes such as downregulation of endocytosis and
55 increased migratory behavior (Garrett et al., 2000; West, Prescott, Eskelinan, Ridley, & Watts,
56 2000). Cytoskeletal remodeling also has a direct impact on the ability of mature DCs to prime T
57 cells (Al-Alwan, Rowden, Lee, & West, 2001; Comrie, Li, Boyle, & Burkhardt, 2015). Indeed,
58 depolymerization of actin filaments perturbs the ability of mature peptide-pulsed DCs to
59 activate T cells, indicating that actin plays an important role on the DC side of the immunological
60 synapse. We hypothesized that maturation-associated changes in the actin cytoskeleton

61 modulate the stiffness of the DC cortex, and **promote T cell priming by providing physical**
62 **resistance to the pushing and pulling forces exerted by the interacting T cell.**

63 In this work, we aimed to better understand the relationship between DC cortical stiffness and T
64 cell activation. We show that **during maturation, DCs undergo a 2-3 fold increase in cortical**
65 **stiffness**, and that T cell activation is sensitive to stiffness over the same range. Stiffness
66 sensitivity was observed in all T cell populations tested, and was **particularly robust in naïve**
67 **CD4⁺ T cells**. Moreover, **stiffness responses were most profound when T cells were engaged**
68 **through TCRαβ directly**, consistent with a mechanosensing mechanism **involving receptor**
69 **deformation**. Since we find that stiffer surfaces lower the threshold signal required for T cell
70 activation, we conclude that stiffness serves as a novel biophysical costimulatory mechanism
71 that functions in concert with canonical signaling cues to facilitate T cell priming.

72 **RESULTS**73 **Dendritic cell stiffness increases upon maturation.**

74 During maturation, DCs undergo a set of phenotypic changes that transform them into highly
75 effective APCs (Mellman & Steinman, 2001). We hypothesized that as part of this maturation
76 process, DCs might also modulate their cortical stiffness. To test this, we used atomic force
77 microscopy (AFM) to directly measure cortical stiffness of immature and mature DCs. Murine
78 bone marrow derived DCs (BMDCs) were prepared as described in Materials and Methods and
79 cultured in the absence or presence of LPS to induce maturation. Cells were plated on Poly L-
80 lysine (PLL) coated coverslips and allowed to spread for at least 4 hours prior to measurement of
81 cortical stiffness by AFM micro-indentation. Because the population of LPS-treated cells was
82 heterogeneous with respect to maturation markers, cells were labeled with fluorescent anti-
83 CD86, and immature (CD86 negative) or mature (CD86 high) cells were selected for AFM
84 measurements (Figure 1 – Supplement 1). As shown in Figure 1A, immature BMDCs were quite
85 soft, with a mean Young's modulus of 2.2 ± 1.7 kPa. **Mature BMDCs were almost two-fold stiffer**,
86 with a Young's modulus of 3.3 ± 1.4 kPa. Importantly, the stiffness of CD86-negative BMDCs
87 within the LPS-treated population was 2.0 ± 1.0 , the same as that of untreated, immature DCs.
88 This demonstrates that the observed increase in stiffness is a property of DC maturation rather
89 than an unrelated response to LPS treatment. Since BMDCs do not recapitulate all of the
90 properties of classical, tissue resident DCs (Guilliams & Malissen, 2015; Lutz, Inaba, Schuler, &
91 Romani, 2016; Na, Jung, Gu, & Seok, 2016), we verified our results by measuring the stiffness of
92 *ex-vivo* DCs purified from spleens of untreated or LPS-injected mice. Results were very similar;
93 the stiffness of immature splenic DCs was 1.9 ± 0.7 , and LPS treatment induced a 2.5 fold increase
94 in stiffness resulting in mature splenic DCs with a mean Young's modulus of 4.8 ± 1.7 kPa. (Figure
95 1B). These results demonstrate that **stiffness modulation is a *bona fide* trait of DC maturation.**

96 Moreover, they establish that the biologically relevant range of DC stiffness lies between 2 and 8
97 kPa.

98 **The maturation-induced increase in stiffness is actin dependent and substrate independent.**

99 One well-known feature of DC maturation is remodeling of the actin cytoskeleton. This process
100 involves changes in the activation status of Rho GTPases and downstream actin regulatory
101 proteins, and is known to downregulate antigen uptake and increase cell motility (Garrett et al.,
102 2000; West et al., 2000). To ask if changes in actin cytoarchitecture also result in increased
103 cortical stiffness, we treated immature and mature BMDCs with the actin-depolymerizing agents
104 Cytochalasin-D or Latrunculin-B. Neither drug affected the stiffness of immature BMDCs,
105 indicating that the basal level of stiffness depends on factors other than the actin cytoskeleton
106 (Figure 1C). In contrast, both drugs induced a significant decrease in the stiffness of mature DCs,
107 with Cytochalasin reducing their stiffness to that of immature DCs. We conclude that the
108 increased cortical stiffness observed upon DC maturation is another feature of **actin cytoskeletal**
109 **reprogramming.**

110 Some cell types regulate their stiffness in response to the stiffness of their substrate (Byfield et
111 al., 2009; Tee, Fu, Chen, & Janmey, 2011). To test whether DCs exhibit this behavior, immature
112 and mature BMDCs were plated on PLL-coated substrates of different compliances (hydrogels of
113 **2 or 25 kPa**, or glass surfaces in the GPa range) and allowed to spread on the surface for at least
114 4 hours prior to AFM measurement. Importantly, when allowed to spread on different PLL-
115 coated surfaces, no notable changes were detected in BMDC morphology, and changes in cell
116 spreading area were minimal (less than 10%, Figure 1 - Supplement 2). Hydrogel compliance was
117 verified by measuring the elastic modulus of the surface in areas devoid of cells (Figure 1 -
118 Figure Supplement 3). As shown in Figure 1D, **substrate compliance had no effect on cortical**
119 **stiffness of either immature or mature BMDCs**. In control studies, we could readily detect

120 substrate-dependent changes in stiffness of normal fibroblast cells (not shown). Thus, we
121 conclude that DCs maintain a specific cortical stiffness, which is characteristic of their
122 maturation state.

123 **DC cortical stiffness is primarily controlled by actin polymerization**

124 We next sought to identify the molecular mechanisms controlling DC cortical stiffness. Several
125 actin regulatory mechanisms are known to change during DC maturation. In particular, mature
126 DCs upregulate the actin bundling protein fascin (Yamashiro, 2012), show activation of myosin-
127 dependent processes (van Helden et al., 2008), and undergo changes in the activation and
128 localization of Rho-GTPases, which in turn regulate actin polymerization via the Arp2/3 complex
129 and formins (Burns, Thrasher, Blundell, Machesky, & Jones, 2001; Garrett et al., 2000; West et
130 al., 2000). To ask how each of these pathways influences cortical stiffness, we used small
131 molecule inhibitors and DCs from relevant knockout mice. Note that to facilitate comparison
132 between experiments, control immature and mature DCs were tested in each experiment, and
133 results were normalized based on values for mature DCs. First, we tested the role of fascin,
134 which is known to generate very stiff actin bundles *in vitro* (Demoulin, Carlier, Bibette, & Baudry,
135 2014). Surprisingly, the stiffness of BMDCs from fascin^{-/-} mice was not significantly different from
136 that of WT BMDCs either before or after LPS-induced maturation (Figure 2A). Next, we tested
137 the contribution of myosin contractility, which is known to control stiffness and membrane
138 tension in other cell types (Salbreux, Charras, & Paluch, 2012). As shown in Figure 2B, treating
139 mature BMDCs with the myosin II inhibitor blebbistatin reduced stiffness by a small, albeit
140 statistically significant amount. Similar results were obtained with the Rho-kinase (ROCK)
141 inhibitor Y27623, which indirectly inhibits myosin function.

142 We next considered the possibility that cortical stiffness is modulated by actin polymerization.
143 Broadly speaking, actin polymerization is induced by two sets of proteins: formins generate

144 linear actin filaments, while activators of the Arp2/3 complex produce branched actin
145 structures. Treatment of DCs with the pan-formin inhibitor SMIFH2 significantly reduced the
146 cortical stiffness of mature DCs (Figure 2B). The most profound reduction was observed after
147 inhibition of Arp2/3-mediated branched actin polymerization by CK666. DCs express multiple
148 activators of Arp2/3 complex, of which two have been implicated in maturation-associated
149 changes in actin architecture: Hematopoietic Lineage Cell-Specific Protein 1 (HS1), the
150 hematopoietic homologue of cortactin (Huang et al., 2011), and WASp, the protein defective in
151 Wiskott-Aldrich syndrome (Bouma, Burns, & Thrasher, 2007; Bouma et al., 2011; Calle, Chou,
152 Thrasher, & Jones, 2004). To individually assess the role of these two proteins, we used BMDCs
153 cultured from HS1 and WASp knockout mice. As shown in Figure 2A, loss of HS1 had no impact
154 on cortical stiffness of either immature or mature BMDCs. In contrast, mature WASp knockout
155 BMDCs were significantly less stiff than WT controls. This difference mirrors that seen after
156 inhibition of Arp2/3 complex by CK666, suggesting that WASp is the primary activator of Arp2/3
157 complex-dependent changes in cortical stiffness. The defect in WASp knockout DCs was
158 observed only after maturation; immature WASp knockout DCs did not differ in stiffness from
159 WT controls. This is consistent with our finding that the stiffness of immature DCs is unaffected
160 by actin depolymerizing agents. Taken together, these results show that activation of WASp-
161 dependent actin polymerization pathway, and to a lesser extent increased myosin contractility
162 and formin mediated actin polymerization, all contribute to the increased cortical stiffness of
163 mature DCs.

164 **Stiffness lowers the threshold for activation of CD4⁺ T cells, but not CD8⁺ T cells.**

165 Our findings raise the possibility that changes in DC cortical stiffness, like other maturation-
166 induced changes, enhance the ability of these cells to prime a T cell response. Previous studies
167 have shown that T cells are sensitive to the stiffness of stimulatory surfaces (Alatoom et al.,

168 2020; Judokusumo et al., 2012; O'Connor et al., 2012), and that that the TCR serves as the
169 mechanosensor (Judokusumo et al., 2012). However, the results are conflicting, and these
170 studies were not performed within the physiological stiffness range that we have defined for
171 DCs. Thus, we tested T cell responses on hydrogels with a stiffness range spanning that of
172 immature and mature DCs (2 – 25 kPa). Compliance of the hydrogel surfaces was verified by
173 measuring the elastic modulus of the surfaces directly by AFM. Hydrogel stiffnesses were found
174 to be similar to those reported by the manufacturer (Figure 3 - Figure Supplement 1). Surfaces
175 were coated with varying doses of peptide-loaded major histocompatibility complex (pMHC)
176 molecules, together with a constant dose of anti-CD28. Surfaces were coated with H-2K^b class I
177 MHC loaded with the N4 (SIINFEKL) peptide (pMHC-I), or I-A^b class II MHC loaded with the
178 OVA₃₂₉₋₃₃₇ (AAHAEINEA) peptide (pMHC-II), to stimulate OT-I CD8⁺ or OT-II CD4⁺ T cells,
179 respectively. Plastic surfaces, which are commonly used for stimulation with surface-bound
180 ligands, were included as a familiar reference point. Importantly, the surface chemistry and
181 ligand binding properties of plastic and hydrogel surfaces are fundamentally different, so direct
182 comparison is not meaningful. To test the effects of substrate stiffness on early T cell activation,
183 we measured surface expression of the activation markers CD25 and CD69, as well as the
184 production of IL-2, all at 24 hours post stimulation. As shown in Figure 3A-C, CD4⁺ T cells showed
185 a profound stiffness-dependent response at 24 hours across all measures. This response was
186 most clearly seen for upregulation of CD25 and CD69, where increasing substrate stiffness
187 enhanced the CD4+ T cell response in a graded manner. As expected, for any given substrate
188 stiffness T cell activation increased with increasing peptide dose. However, comparison among
189 stimulatory surfaces revealed that increasing substrate stiffness lowered the pMHC-II dose
190 required to obtain the same level of activation. Over the stiffness range associated with DC
191 maturation (2-8kPa), the dose of TCR signal needed to induce surface marker upregulation was
192 shifted by 1-2 logs. Analysis of IL-2 production revealed a similar effect, although the stiffness

193 sensitivity was more bi-modal. IL-2 production increased almost 3-fold when CD4+ T cells were
194 stimulated on surfaces of **8kPa**, as opposed to **2kPa**, for the same antigen dose.

195 Strikingly, the robust stiffness response we observed in CD4⁺ T cells was **not recapitulated for**
196 **CD8⁺ T cells**, especially when T cell activation was assessed based on surface marker
197 upregulation (Figure 3D,E). Analysis of IL-2 production did reveal stiffness-enhanced activation
198 of naïve CD8⁺ T cells; as in CD4⁺ T cells, this was clearest across the stiffness range associated
199 with DC maturation. To determine if the stiffness dependency of CD4⁺ T cells seen at early times
200 after TCR engagement is maintained at later times, we measured T cell proliferation based on
201 CFSE dilution at 72 hours post stimulation. Similar to what was observed for early activation
202 markers, increasing substrate stiffness produced graded increases in CD4⁺ T cell proliferation,
203 and the threshold dose required to induce robust proliferation shifted as a function of substrate
204 stiffness (Figure 4A,B). This effect was particularly evident at low doses of pMHC-II (0.1-1ug/ml).
205 Interestingly, although soft hydrogels (2-4 kPa) elicited only very low levels of CD4⁺ T cell
206 proliferation, these substrates did induce upregulation of CD25 in a high percentage of CD4⁺ T
207 cells, even in the undivided populations (Figure 4C,D). This indicates that an activating signal was
208 received, but was insufficient to drive proliferation.

209 Since the threshold stimuli (stiffness and dose of pMHC-II) required to induce significant IL-2
210 production and proliferation were very similar (Figures 3C and 4B), we reasoned that the
211 threshold for proliferation might be driven by IL-2 availability. To test this, OT-II CD4⁺ T cells
212 were stimulated on hydrogels with or without addition of 25 U/ml exogenous IL-2. Interestingly,
213 addition of IL-2 did not rescue the proliferation of T cells stimulated on soft surfaces, nor did it
214 increase proliferation on stiffer ones (Figure 4E). Thus, we conclude that in addition to
215 influencing the signaling threshold for IL-2 production, substrate stiffness also affects other IL-2
216 independent events needed for efficient T cell proliferation.

217 Although early activation events in CD8⁺ T cells showed little to no stiffness sensitivity, CD8⁺ T
218 cells showed mild stiffness-dependent proliferation (Figure 5A,B). The concentration of
219 stimulatory ligand needed to induce at least one round of division was similar across the entire
220 stiffness range Over successive rounds, increased stiffness did enhance the extent of
221 proliferation, but the differences were relatively small (Figure 5B). Interestingly, analysis of CFSE
222 dilution as a function of CD25 expression reveals evidence that CD8⁺ T cells exhibit a binary
223 stiffness response (Figure 5 C,D); at low doses of peptide ligand, cells stimulated on very stiff
224 substrates (25kPa or plastic) survived and proliferated, whereas cells stimulated on softer
225 substrates were mostly lost (Figure 5C). From the standpoint of T cell priming, the significance of
226 this observation is unclear, since these stiffnesses are well outside the biologically relevant
227 range we measured for DCs.

228 The observed difference between CD4 and CD8 T cell stiffness response could be associated
229 with the difference in antigen strength between the AAHAEINEA (OVA₃₂₃₋₃₃₉) pMHC-II complex
230 used to stimulate CD4⁺ T cells, and the SIINFEKL (N4) pMHC-I complex used to stimulate CD8⁺ T
231 cells. To verify that this is not the case, both CD4⁺ and CD8⁺ T cells were stimulated in the same
232 way, using surfaces of different stiffness with varying concentrations of αCD3ε together with 2
233 µg/ml of αCD28. Proliferation was measured based on CFSE dilution at 72 hours post stimulation
234 (Figure 5 – Supplement 1). We found that even when both are stimulated through the CD3
235 complex, CD4⁺ T cells exhibit profound stiffness sensitivity (especially within the physiological
236 range), while the stiffness responses of CD8⁺ T cells are more modest. Thus, we conclude that
237 the more robust stiffness response of CD4⁺ vs CD8⁺ T cells stems from differences in the cells
238 themselves, rather than the properties of the particular pMHC / TCR pairs used for investigation.

239 Taken together, our findings point to a mechanism in which stiffer substrates have a sensitizing
240 effect on CD4⁺ T cells, similar to that of classical co-stimulatory molecules such as CD28

241 (Harding, McArthur, Gross, Raulet, & Allison, 1992). When considered in this way, the relative
242 lack of stiffness responses in CD8⁺ T cells fits with the fact that CD8⁺ T cells are much less
243 dependent on costimulatory signals (McAdam, Schweitzer, & Sharpe, 1998).

244 **Degranulation of cytotoxic T cells shows mild stiffness sensitivity.**

245 Whereas naïve T cells are activated by DCs, effector T cells interact with many cell types. In
246 particular, cytotoxic CD8⁺ T cells (CTLs) must respond to a variety of possible target cells, which
247 may differ widely with respect to stiffness. We therefore reasoned that CTL effectors might be
248 stiffness independent. To test this, we measured the extent of cytotoxic granule release
249 (degranulation) of effector OTI CTLs stimulated on different stiffness hydrogel surfaces. CTLs
250 were re-stimulated on hydrogels coated with a range of pMHC-I concentrations in the presence
251 of fluorescent anti-CD107a antibody and the amount of CD107a on the cell membrane was
252 analyzed by flow cytometry. Degranulation showed only a mild stiffness dependency (Figure 5E),
253 and stiffness tended to affect the magnitude of degranulation rather than whether or not a
254 degranulation response was triggered. Interestingly, changes in substrate stiffness within the
255 range of defined for DCs (2-8kPa) had little or no impact on degranulation. Increased
256 degranulation was only seen on stiffer surfaces (12 and 25 kPa). This could have functional
257 consequences for effector function *in vivo*, since target cells in inflamed tissues can reach this
258 stiffness range.

259 **Engagement of the TCR complex by pMHC elicits the most prominent stiffness response**

260 Many current models for TCR mechanosensing are founded on the notion of TCR deformation
261 following engagement of cognate pMHC (Ma, Janmey, & Finkel, 2008). According to this
262 concept, forces applied by the T cell on the TCR-pMHC bond result in conformational changes
263 within TCR $\alpha\beta$ (primarily the β chain), which are transmitted to intracellular components of the
264 TCR/CD3 complex, leading to the initiation of downstream signaling (Das et al., 2015; Lee et al.,

265 2015; Swamy et al., 2016). Given this, we wondered whether engaging the TCR complex through
266 the CD3 ϵ chain, as compared to direct TCR $\alpha\beta$ engagement, would differentially affect T cell
267 mechanosensing. To test this, CD4 $^{+}$ OT-II T cells were stimulated on hydrogels coated with anti-
268 CD3 ϵ antibodies, anti-TCR β antibodies, or pMHC-II monomers. T cell activation was measured at
269 72 hours based on proliferation (CFSE dilution) and expression of CD25 (Figure 6). All three
270 ligands induced a stiffness-dependent response for both proliferation and CD25 expression, but
271 the responses differed in significant ways. In general, stimulating T cells with pMHC-II resulted in
272 the strongest responses on the hydrogel surfaces; only on plastic surfaces did anti-CD3 ϵ
273 stimulation yield a similarly strong response (Figure 6A,C). Importantly, on surfaces with a
274 stiffness similar to that of mature DCs (8kPa), stimulation with pMHC resulted in robust
275 proliferation, while stimulation with anti-CD3 ϵ yielded a minimal response. On softer substrates
276 (2-4kPa), pMHC elicited some proliferation, whereas stimulation with anti-CD3 did not.
277 Interestingly, stimulation with anti-TCR β resulted in a mixed response. At high doses of antigen,
278 stimulation with anti-TCR β yielded clear proliferative responses on substrates within the
279 biologically-relevant stiffness range. Analysis of CD25 expression patterns revealed a similar
280 trend (Figure 6D-F); on soft surfaces, pMHC yielded the strongest response, and anti-TCR β was
281 more effective than anti-CD3 ϵ . Taken together, these results indicate that T cells sense substrate
282 stiffness best through direct engagement of TCR $\alpha\beta$ as predicted by the receptor deformation
283 model.

284 **The increased stiffness of mature DCs enhances their ability to prime T cells**

285 Our hydrogel assays show that T cell activation is enhanced by changes in stiffness over the
286 range observed for DC maturation, consistent with the idea that modulation of cortical stiffness
287 is a biophysical mechanism by which DCs control T cell activation. To test this directly, we sought
288 conditions under which we could manipulate the stiffness of mature DCs. We took advantage of

289 our finding that mature WASp-KO BMDCs are approximately 20% softer than WT controls
290 (Figure 2A; data are presented as absolute values in Figure 7A). WT and WASp-KO BMDCs were
291 pulsed with increasing concentrations of OVA₃₂₃₋₃₃₉ peptide and used to prime OT-II CD4⁺ T cells.
292 As shown in Figure 7B, WASp-KO BMDCs did not prime T cells as efficiently as WT BMDCs at low
293 OVA concentrations. Higher concentrations of OVA rescued this defect, showing that loss of
294 WASp shifts the dose of peptide needed rather than affecting T cell priming *per se*, in keeping
295 with the view that DC stiffness provides a costimulatory signal. We next attempted to test T cell
296 priming activity of DCs that are stiffer than WT cells. We tested several genetic manipulations,
297 most of which did not significantly increase the cortical stiffness of mature BMDCs. We did find
298 that overexpression of a constitutively active form of WASp (I294T, CA-WASp (Beel et al., 2009))
299 increased cortical stiffness of mature BMDCs by approximately 20% relative to WT cells (Figure
300 7A), but these BMDCs failed to prime T cells more efficiently (Figure 7C). Expression of CA-WASp
301 only enhances BMDC stiffness to approximately 5kPa, and based on our hydrogel studies, this
302 increase is unlikely to be sufficient to enhance T cell activation. It seems likely that conditions
303 that stiffen DCs to 10kPa or more would further enhance T cell responses, but we were unable
304 to test this directly, and it is not clear whether this happens *in vivo*. Nonetheless, the studies
305 using WASp-KO DCs show that changes in DC stiffness impact their ability to efficiently prime a
306 T cell response.

307 **DISCUSSION**

308 Recent work from several labs clearly shows that T cell activation involves mechanical cues
309 (Reviewed in (Blumenthal & Burkhardt, 2020)). We have previously shown that the DC
310 cytoskeleton constrains the mobility of stimulatory ligands on the DC surface, enhancing T cell
311 activation by opposing the forces exerted by the T cell on the corresponding receptors (Comrie
312 et al., 2015). In the current study, we elucidate a second mechanism whereby the DC

313 cytoskeleton enhances T cell activation. We show that actin remodeling during DC maturation
314 increases the cortical stiffness of DCs by 2-3 fold, and that T cell activation is enhanced by
315 increases in stiffness over the same range. Importantly, increased stiffness lowers the threshold
316 dose of TCR ligand needed for T cell activation, as expected if substrate stiffness serves as a
317 costimulatory signal. In keeping with this concept, CD4⁺ T cells showed more profound stiffness-
318 sensitivity than CD8⁺ T cells, especially at early times in the activation process. Together, these
319 results indicate that stiffening of the DC cortex during maturation provides biophysical cues that
320 work together with canonical costimulatory cues to enhance T cell priming.

321 Modulation of actin architecture has long been appreciated as an essential feature of DC
322 maturation. Changes in the DC actin cytoskeleton facilitate the transition from highly endocytic
323 tissue-resident cells to migratory cells specialized for antigen presentation (Burns et al., 2004;
324 Burns et al., 2001). Our findings reveal a new facet of this process. We show that immature DCs
325 are very soft, and that upon maturation, their cortical stiffness is increased by 2-3 fold. This is
326 true for cultured BMDCs treated with LPS *in vitro*, as well and splenic DCs harvested from LPS-
327 treated mice. A similar trend was reported by Bifi et al for human monocyte-derived DCs (Bifi
328 et al., 2015), although that study reported lower absolute Young's modulus values. While we
329 used AFM indentation, Bifi et al. used microplate rheology. Since different methods for
330 measuring cell mechanical properties produce absolute Young's modulus values that can vary by
331 as much as 100 fold (Wu et al., 2018), it seems likely that the apparent discrepancy in absolute
332 values stems from technical differences between the two studies. Nevertheless, it is clear from
333 both studies that the stiffness of the DC cortex is modulated during maturation.

334 It is important to note that DCs have complex surface topologies with prominent invaginations
335 and projections that change dramatically during maturation (Knight et al., 1986; Verdijk et al.,
336 2004). In particular, mature DCs exhibit characteristic membrane veils, as well as microvilli-rich

337 regions that serve as preferred docking sites for T cells (Fisher, Bulur, Vuk-Pavlovic, Prendergast,
338 & Dietz, 2008). This complexity makes the interpretation of AFM measurements of cortical
339 stiffness more challenging, as measuring stiffness on a protrusive veil may yield a different result
340 than measuring stiffness directly over the cell body. Because these different structures cannot
341 be resolved by light microscopy we were unable to test for regional stiffness differences (apart
342 from avoiding the nucleus of the cell). Importantly, there were very few instances where
343 measurement of stiffness at two different locations of the same cell resulted in significantly
344 different values (data not shown). Going forward, it will be interesting to determine whether the
345 area of the DC cortex directly underlying an interacting T cell has distinct stiffness properties,
346 and whether this represents a feature of T cell docking sites, or a localized effect of T cell
347 interaction on the DC cytoskeleton.

348

349 The observed increase in stiffness depends on changes in actin architecture; whereas
350 depolymerization of actin filaments has no effect on the stiffness of immature DCs, the increase
351 associated with maturation depends on intact filaments, and is sensitive to inhibitors of actin
352 polymerizing molecules. While it remains to be determined exactly which actin regulatory
353 pathways control cortical stiffness in mature DCs, our data show that both Arp2/3 complex and
354 formins are involved. Moreover, we find that DCs lacking the Arp2/3 activator WASp are
355 abnormally soft. In keeping with these findings, DC maturation is known to induce changes in
356 the activation state and localization of Rho family GTPases, especially Cdc42, a molecule that
357 can activate both WASp and formins (Garrett et al., 2000; Vargas et al., 2016; West et al., 2000).
358 Since the overall levels of active Cdc42 are diminished during DC activation, it seems likely that
359 the observed increase in cortical stiffness results from redistribution of the active pool.

360 We show that DC cortical stiffness is a cell-intrinsic property that is unaffected by substrate
361 stiffness. In this respect, DCs are different from other cell types that adapt their stiffness to
362 differences in substrate compliance (Byfield et al., 2009; Tee et al., 2011). The ability of DCs to
363 maintain constant stiffness despite changing environmental cues is reminiscent of previous work
364 showing that DCs rapidly change their method of locomotion in order to maintain consistent
365 migration speed and shape while crossing over different surfaces (Renkawitz et al., 2009). This
366 behavior has been proposed to allow DCs to pass through tissues with widely different
367 mechanical properties. In the same way, we propose that the ability of DCs to regulate cortical
368 stiffness as a function of maturation state in spite of environmental cues reflects the importance
369 of this property for priming an appropriate T cell response.

370 A central finding of this paper is that changes in DC stiffness serves as a costimulatory signal for
371 T cell priming. By using a matrix of different hydrogels spanning the biologically relevant range
372 defined for immature and mature DCs (2 – 8 kPa), coated with increasing pMHC concentrations,
373 we found that stimulatory substrates with higher stiffness required lower concentrations of
374 pMHC to achieve T cell activation. Similarly, when compared to WT DCs, softer WASp knockout
375 DCs required higher concentrations of OVA peptide to induce the same level of proliferation.
376 Our results indicate that increases in cortical stiffness, together with diminished ligand mobility
377 (Comrie et al., 2015), represent biophysical cues that are modulated in parallel with
378 upregulation of costimulatory ligands and cytokines as a fundamental part of DC maturation.
379 When interacting T cells engage pMHC complexes and costimulatory ligands on the DC surface,
380 they integrate this biophysical input along with other canonical costimulatory signals.
381 In addition to lowering the antigenic threshold for T cell activation, changes in stiffness may
382 present a new signaling mechanism by which DCs control T cell fate and differentiation. Bufl et
383 al. showed previously that human monocyte-derived DCs responding to different maturation

384 signals vary in their stiffness (Bufl et al., 2015). Interestingly, they found that treatment with the
385 tolerizing cytokines TNF α and prostaglandin E2 results in DCs that are even softer than
386 immature cells. Tolerogenic DCs exhibiting partially immature phenotypes have been shown to
387 induce differentiation of regulatory T cells (Doan, McNally, Thomas, & Steptoe, 2009; Gleisner,
388 Rosemblatt, Fierro, & Bono, 2011; Gordon, Ma, Churchman, Gordon, & Dawicki, 2014). This
389 effect is usually attributed to low expression of T cell ligands or cytokines, but based on our
390 data, we propose that biophysical properties of the DC cortex also play a role. Going forward, it
391 will be important to ask how DC stiffness is modulated in response to different environmental
392 cues, and whether this further shapes T cell responses.

393 While we demonstrate T cell stiffness responses on soft surfaces emulating DCs, others have
394 reported T cell stiffness responses on very stiff surfaces (Judokusumo et al., 2012; O'Connor et
395 al., 2012). We found that very stiff substrates (25kPa hydrogels and plastic surfaces in the GPa
396 range) elicit strong responses. This was true for proliferation, IL-2 secretion and degranulation.
397 Similarly, recent analysis of human CD4 $^{+}$ effector T cells shows that re-stimulation on soft
398 surfaces induces upregulation of genes related to cytokine signaling and proliferation, while
399 restimulation on very stiff surfaces (100 kPa) triggers expression of an additional genetic
400 program that includes metabolic proteins related to glycolysis and respiratory electron transport
401 (Saitakis et al., 2017). The physiological relevance of these augmented responses is unclear,
402 since T cells probably never encounter such stiff stimulatory surfaces *in vivo*. Nonetheless, such
403 findings raise important questions about traditional *in vitro* assays of T cell function, which often
404 utilize glass or plastic stimulatory surfaces.

405 The observation that T cells respond to APC stiffness is best understood in the context of
406 evidence that T cells exert force on an interacting APC through the TCR complex (Bashour et al.,
407 2014; Blumenthal & Burkhardt, 2020; Hui et al., 2015; Husson et al., 2011; Li et al., 2010;

408 Sawicka et al., 2017), with the amount of force corresponding to APC stiffness (Husson et al.,
409 2011; Sawicka et al., 2017). Apart from being a requirement for activation (Li et al., 2010;
410 Pryshchep et al., 2014), force transduction has been shown to promote peptide discrimination
411 by influencing bond lifetimes (Das et al., 2015; Liu et al., 2014). Importantly, it appears that the
412 TCR's ability to sense stiffness is closely related to its ability to transduce force-dependent
413 signals during T cell-APC interaction. Indeed, there is evidence that signaling downstream of TCR
414 engagement is increased on stiffer substrates (Alatoom et al., 2020; Judokusumo et al., 2012)
415 and that the intracellular location of early tyrosine phosphorylation events corresponds to sites
416 of maximum traction force (Bashour et al., 2014). We propose that stiffer substrates allow T
417 cells to exert more force through TCR interactions, and consequently induce more effective
418 signaling. This accounts for the co-stimulatory property of substrate stiffness on T cell activation.

419 The mechanism by which force application on the TCR is translated into biochemical signals
420 remains controversial. Nevertheless, there is evidence to suggest that force applied on the TCR
421 complex induces conformational changes within TCR $\alpha\beta$ that exposes ITAM sites on the CD3 and
422 TCR ζ chains for phosphorylation and downstream signaling (Lee et al., 2015; Swamy et al., 2016)
423 Importantly, conformational changes are mainly attributed to extension of the C β FG loop region
424 within TCR β (Das et al., 2015), which serves as a lever to push down on the CD3 complex (Sun,
425 Kim, Wagner, & Reinherz, 2001), exposing ITAM sites (Xu et al., 2008). In support of this idea, we
426 found that the way in which the TCR is engaged influences T cell stiffness sensing. Within the
427 biologically relevant stiffness range (2-8 kPa), T cells were activated only when TCR $\alpha\beta$ was
428 engaged directly; indirect engagement through anti-CD3 resulted in almost no response. We
429 postulate that direct TCR $\alpha\beta$ engagement leads to conformational changes that are transmitted
430 appropriately for efficient initiation of downstream signaling, whereas engagement of CD3
431 induces smaller changes and more limited downstream signaling. This effect may be most

432 evident on soft substrates, because force-dependent signaling is limiting in this setting. We note
433 that on these soft substrates, pMHC induced stronger T cell activation than anti-TCR β . This may
434 reflect the involvement of CD4 in the former, which leads to more efficient recruitment of Lck to
435 the TCR complex. One caveat to our work is that pMHC complexes are immobilized on the
436 hydrogel surfaces used here, whereas pMHC complexes show relatively high lateral mobility in
437 the DC membrane, even after maturation (Comrie et al., 2015). Future studies addressing how
438 the biophysical properties of the DC surface contribute to tension on the TCR and receptor
439 deformation will need to address the relationship between stiffness and mobility.

440 Although our focus here is on the role of stiffness sensing in priming of naïve T cells, we find that
441 effector CD8 $^+$ T cells also exhibit stiffness-dependent degranulation; stiffness-dependent
442 cytokine production by CTLs has also recently been reported (Tello-Lafoz et al., 2020). Similarly,
443 Saitakis et al. have shown that restimulating CD4 $^+$ effector T cells on surfaces of different
444 stiffness induces differential gene expression and cytokine production (Saitakis et al., 2017).
445 Since DCs increase their cortical stiffness during maturation, a stiffness dependent mechanism
446 for naïve T cell priming makes biological sense. Effector T cells, however, interact with a variety
447 of APCs. In particular, cytotoxic CD8 $^+$ T cells are expected to kill any infected cell throughout the
448 body with no stiffness bias. The physiological significance of stiffness sensitivity for effector T
449 cells remains unclear. It's possible that mechanosensing is not needed for effector function per
450 se, but that it is an obligate component of the feedback loop that underlies force-dependent
451 TCR triggering.

452 The IS is often described as a platform for information exchange between the T cell and APC.
453 Together with our recent work on ligand mobility, the findings presented here indicate that the
454 mechanical properties of the APC side of the IS influence T cell priming, likely because they
455 augment force-dependent conformational changes in TCRs, integrins, and potentially other

456 molecules. Going forward, it will be important to determine how these properties are
457 modulated during DC maturation, and whether there are also local changes induced by signaling
458 events taking place at the IS. In addition, it will be important to tease apart the molecular events
459 through which T cells sense and respond to these mechanical cues.

461 Key Resource Table

Reagent type (species) or resource	Designation	Source or reference	Identifiers	Additional information
antibody	APC/APC-Cy7 anti-CD4 (rat, clone GK1.5)	Biolegend	Biolegend:100411/10041; RRID:100411/AB_312698	Flow (1:350)
antibody	APC/PE-Cy7 anti-CD8a (rat, clone 53-6.7)	Biolegend	Biolegend: 00711/100721; RRID:AB_312750/AB_312760	Flow (1:350)
antibody	anti-CD3ε (A. hamster, clone 145-2C11)	BioXCell	BioXcell: BE0001-1; RRID: AB_1107634	0.003 µg/mL - 10 µg/mL
antibody	anti-CD28 (Syrian hamster, clone PV1)	BioXCell	BioXcell:BE0015-5; RRID:AB_1107628	1 µg/mL - 2 µg/mL
antibody	Anti-CD86 (rat, clone GL-1)	BioXCell	BioXcell: BE0025; RRID: AB_1107678	Stain (1:100)
antibody	Alexa647 anti-CD86 (rat, clone GL-1)	BioLegend	BioLegend: 105020; RRID: AB_493464	Stain (1:100)
antibody	APC-Cy7 anti-CD86 (rat, clone GL-1)	BioLegend	BioLegend:105029; RRID:AB_2074993	Flow (1:100)
antibody	Anti I-A/I-E (rat, clone M5/114)	BioXCell	BioXcell:BE0108-5; RRID:AB_10949298	Stain (10 µg/ml)
antibody	PE anti- I-A/I-E (rat, clone M5/114.15.2)	BioLegend	BioLegend:107607; RRID:AB_313322	Flow (1:100)
antibody	APC anti-CD11c (rat, clone N418)	BioLegend	BioLegend:117309; RRID:AB_313778	Flow (1:100)
antibody	PE-antiCD107a (LAMP-1) (rat, clone 1D4B)	BioLegend	BioLegend:121611; RRID:AB_1732051	Assay (2 µg/mL)
antibody	Alexa680 goat anti-Rat IgG (H+L)	ThermoFisher	ThermoFisher: A-21096 RRID: AB_2535750	Stain (1:500)
chemical compound, drug	Cytchalasin-D	EMD Millipore	EMD Millipore: 250255; CAS:22144-77-0	10 µM
chemical compound, drug	Latrunculin-B	EMD Millipore	EMD Millipore: 428020; CAS:76343-94-7	10 µM
chemical compound, drug	(S)-nitro-Blebbistatin	Cayman Chemical	Cayman Chemical:13891; CAS:856925-75-2	50 µM
chemical compound, drug	CK666	EMD Millipore	Millipore: 182515; CAS:442633-00-3	100 µM

chemical compound, drug	Y27632	SIGMA	SIGMA:688000; CAS:146986-50-7	25 µM
chemical compound, drug	SMIFH2	SIGMA	SIGMA:344092; CAS:340316-62-3	10 µM
chemical compound, drug	Escherichia coli 026:B6; LPS	SIGMA	SIGMA:L2762; ECN:297-473-0	200 ng/mL
chemical compound, drug	Collagenase D	SIGMA	SIGMA: COLLD-RO; EC#:3.4.25.3	2 mg/mL
chemical compound, drug	IL-2	NIAID, NIH	N/A	25U;100U
chemical compound, drug	streptavidin-coated polystyrene beads	Spherotech	Spherotech: SVP-60-5	
chemical compound, drug	EZ-link NHS biotin kit	Thermo Fisher Scientific	Thermo Fisher Scientific: 21217	
chemical compound, drug	CFSE	Invitrogen	Invitrogen: C34570	
commercial assay or kit	CF555 Mix-n-Stain	Biotium	Biotium:92234	
commercial assay or kit	MACS pan-dendritic cell isolation kit	Miltenyi Biotec	Miltenyi: 130-100-875	
commercial assay or kit	mouse IL-2 ELISA kit	Invitrogen	Invitrogen: 88-7024-88	
gene (mouse)	Was; Wiskott–Aldrich syndrome gene	DOI:10.1084/jem.20091245	MGI:105059; NCBI Gene: 22376	
other	Hydrogel surfaces (96 well plates)	Matrigen	EasyCoat Softwell 96G	Customized plates
other	AFM 1 µM spherical polystyrene probe	Novascan	Novascan: PT.PS	Si ₃ N ₄ cantilever k=0.06 N/m
peptide, recombinant protein	Peptide MHC-II Complex	NIH Tetramer Core	I-A ^b	Sequence: HAAHAEINEA
peptide, recombinant protein	Ovalbumin 323–339; OVA _{323–339}	Anaspec	Anaspec: AS-27025; LOT:1755317	Sequence: ISQAVHAAHAEIN EAGR
recombinant DNA reagent	pLX301 (plasmid)	Addgene	Addgene: 25895; RRID: Addgene_25895	DOI:10.1038/nmeth.1638
software, algorithm	FlowJo	FlowJo LLC	RRID:SCR_008520	

software, algorithm	NanoScope Analysis	Broker	N/A	
strain, strain background (Mice)	OT-II Transgenic mice / OT-II	Jackson Laboratories	Stock: 004194; RRID:IMSR_JAX:004194	B6.Cg-Tg(TcraTcrb)425 Cbn/J
strain, strain background (Mice)	OT-I Transgenic mice / OT-I	Jackson Laboratories	Stock: 003831; RRID:IMSR_JAX:003831	C57BL/6-Tg(TcraTcrb)110 0Mjb/J
strain, strain background (Mice)	<i>Was</i> ^{-/-} ; WASP-, WASp-KO	Jackson Laboratories	Stock: 003292; RRID: IMSR_JAX:003292	129S6/SvEvTac- <i>Was</i> ^{tm1Sbs} /J
strain, strain background (Mice)	<i>Hcls1</i> ^{-/-} ; HS1-KO	David Rawlings, MD.	PMCID: PMC394441	
strain, strain background (Mice)	<i>Fscn1</i> ^{-/-}	KOMP Repository, UC Davis	MGI:5605764	<i>Fscn1</i> ^{tm1.1(KOMP)Vlcg}

462 **Inhibitors and antibodies**

463 Cytochalasin-D and Latrunculin-B were from EMD Millipore, (S)-nitro-Blebbistatin was from
 464 Cayman Chemical, CK666 was from Calbiochem, and Y27632 and SMIFH2 were from Sigma-
 465 Aldrich. Flow cytometry antibodies: rat anti-CD4 APC/APC-Cy7 (clone RM4-5), rat anti-CD8a
 466 APC/PE-Cy7 (clone 53-6.7), Armenian hamster anti-CD69 APC (clone H1.2F3) and rat anti-CD25
 467 PE (clone PC61) were all from BioLegend. Surface coating antibodies: Armenian hamster anti-
 468 CD3 ϵ (clone 2C11), and Armenian hamster anti-CD28 (Clone PV1) were from BioXCell.
 469 Biotinylated Armenian hamster anti-CD3 ϵ (clone 2C11) was from Invitrogen, and biotinylated
 470 mouse anti-TCRV β 5.1/5.2 (clone MR9-4) was from BD Bioscience. Dendritic cell staining: anti-
 471 CD86 CF555 was made by conjugating purified rat anti-CD86 (BioXCell) with CF555 conjugated
 472 dye from Biotium as per the manufacturer's protocol.

473 **Mice**

474 All mice were originally obtained from The Jackson Laboratory and housed in the Children's
 475 Hospital of Philadelphia animal facility, according to guidelines put forth by the Institutional
 476 Animal Care and Use Committee. C57BL/6 mice (WT) were purchased from Jackson Labs. HS1-
 477 KO mice on the C57BL/6 background have been previously described(Taniuchi et al., 1995) and

478 were a kind gift from doctor David Rawlings at the University of Washington. *Was*^{-/-} mice were
479 purchased from Jackson labs (Snapper et al., 1998) and fully backcrossed to a C57BL/6
480 background. All mouse strains were used as a source of bone marrow from which to generate
481 BMDCs. Mice bearing a gene trap mutation in the *Fscn1* gene (*Fscn1*^{tm1(KOMP)Vlcg}), which
482 abrogates expression of the protein Fascin 1, were generated by the KOMP Repository at UC
483 Davis, using C57BL/6 embryonic stem cells generated by the Texas A&M Institute for Genomic
484 Medicine. Because these mice proved to have an embryonic lethal phenotype, fetal liver
485 chimeras were used as a source of bone marrow precursors. Heterozygous mating was
486 performed, and fetal livers were collected after 15 days of gestation and processed into a single-
487 cell suspension by mashing through a 35-µm filter. Embryos were genotyped at the time of
488 harvest. Cells were resuspended in freezing media (90% FCS, 10% DMSO) and kept at -80 °C
489 until used. Thawed cells were washed, counted, resuspended in sterile PBS and injected i.v. into
490 sub-lethally irradiated 6-week-old C57BL/6 recipients, 1 × 10⁶ cells per mouse. Chimeras were
491 used as a source for fascin KO bone marrow ~6 weeks after transfer. OT-I T cells were prepared
492 from heterozygous OT-I TCR Tg mice, which express a TCR specific for ovalbumin 257-264
493 (amino acid sequence SIINFEKL) presented on H-2K^b (Hogquist et al., 1994). OT-II T cells were
494 prepared from heterozygous OT-II TCR Tg mice, which express a TCR specific for ovalbumin 323–
495 339 (amino acid sequence ISQAVHAAHAEINEAGR) presented on I-A^b (Barnden, Allison, Heath, &
496 Carbone, 1998).

497 **Cell culture**

498 Unless otherwise specified, all tissue culture reagents were from Invitrogen/Life Technologies.
499 GM-CSF was produced from the B78H1/GMCSF.1 cell line (Levitsky et al., 1996). HEK-293T cells
500 (ATCC) were cultured in DMEM supplemented with 10% FBS, 25mM Hepes,
501 penicillin/streptomycin, GlutaMAX, and non-essential amino acids.

502 Generation of bone marrow derived dendritic cells (BMDCs) was similar to (Inaba et al., 1992).
503 Briefly, mouse long bones were flushed with cold PBS, the resulting cell solution was passed
504 through a 40 µm strainer, and red blood cells were lysed by ACK lysis. Cells were washed once
505 with RPMI-1640 and then either frozen for later use in RPMI-1640 containing 20% FBS, 10%
506 DMSO, or plated in 10 cm bacterial plates in BMDC culture media (RPMI-1640, 10% FBS,
507 penicillin/streptomycin, GlutaMax and 1% GM-CSF supernatant). On day 3 of culture, dishes
508 were supplemented with 10 ml of BMDC culture media. On Day 6, 10 ml of media were
509 replaced, by carefully collecting media from the top of the dish and slowly adding fresh media.
510 BMDC differentiation was verified by flow cytometry, showing 80-90% CD11c positive cells.
511 BMDC maturation was induced on days 7 or 8; immature BMDCs were harvested and re-plated
512 in a 6cm tissue culture dish in 5 ml of BMDC media supplemented with 200 ng/ml LPS
513 (*Escherichia coli* 026:B6; Sigma-Aldrich) for at least 24h. Maturation was verified by flow
514 cytometry, with mature BMDCs defined as Live/CD11c⁺/CD86^{high}/MHC-II^{High} cells. To generate
515 splenic DCs, spleens from C57BL/6 mice were cut to smaller pieces and digested with
516 Collagenase D (2 mg/ml, Sigma) for 30 min at 37°C, 5%CO₂. Cells were washed and labeled for
517 separation by negative selection using a MACS pan-dendritic cell isolation kit (Miltenyi Biotec).

518 Primary mouse T cells were purified from lymph nodes and spleens using MACS negative
519 selection T cell isolation kits (Miltenyi Biotec). In the case of CD4⁺ T cells, ex vivo cells were used.
520 Since isolation yielded mostly naïve cells (> 90%, data not shown), we refer to them as naïve
521 CD4⁺ T cells. In the case of CD8⁺ T cells, approx. 45% of T cells isolated from OT-I mice showed
522 some level of activation. Thus, we specifically isolated naïve T cells by MACS purification. To
523 generate cytotoxic CD8⁺ T cells (CTLs), purified murine CD8⁺ cells were activated on 24-well
524 plates coated with anti-CD3ε and anti-CD28 (2C11 and PV1, 10µg/ml and 2 µg/ml respectively)
525 at 1x10⁶ cells per well. After 24h, cells were removed from activation and mixed at a 1:1 volume

526 ratio with complete T cell media (DMEM supplemented with penicillin/streptomycin, 10% FBS,
527 55μM β-mercaptoethanol GlutaMAX, and non-essential amino acids), containing recombinant
528 IL-2 (obtained through the NIH AIDS Reagent Program, Division of AIDS, NIAID, NIH from Dr.
529 Maurice Gately, Hoffmann - La Roche Inc (Lahm & Stein, 1985)), to give a final IL-2 concentration
530 of 100 units/ml. Cells were cultured at 37°C and 10% CO₂, and passaged as needed to be kept at
531 0.8x10⁶ cells/ml for 7 more days. CTLs were used at days 8 or 9 after activation.

532 **Plasmid construction, viral production, and transduction of DCs:**

533 A constitutively active form of WASp (CA-WASp) was engineered by subcloning WASp cDNA into
534 a pLX301 vector (Addgene), introducing an I294T point mutation (Westerberg et al., 2010) by
535 site-directed mutagenesis, and confirming by sequencing. To generate recombinant lentivirus,
536 HEK-293T cells were co-transfected using the calcium phosphate method with psPAX2 and
537 pMD2.G, together with the DNA of interest in pLX301. For transduction, BMDCs were plated in
538 untreated 6 well plates at 2x10⁶ cells/well in 3 ml of BMDC media. BMDC transduction was
539 carried out on day 2 of culture; lentiviral supernatants were harvested from HEK-293T cells 40hr
540 post transfection, supplemented with 8 μg/ml Polybrene (Sigma-Aldrich), and used immediately
541 to transduce BMDCs by spin-infection at 1000xG, 37°C for 2hr. After resting the cells for 30 min
542 at 37°C, 5% CO₂, lentivirus-containing media was replaced with normal BMDC culture media. On
543 day 5 of culture, puromycin (Sigma-Aldrich) was added to a final concentration of 2 μg/ml to
544 allow selection of transduced BMDCs. Maturation of transduced cells was induced on day 8 by
545 adding 200 ng/ml of LPS in puromycin-free media.

546 **Flow Cytometry**

547 All cells were stained with Live/Dead aqua (ThermoFisher) following labeling with appropriate
548 antibodies in FACS buffer (PBS, 5% FBS, 0.02% NaN₃, and 1 mM EDTA). Flow cytometry was
549 performed using either the Cytoflex LX or CytoFlex S cytometer (Beckman Coulter) and analyzed

550 using FlowJo software (FlowJo LLC). T cells were gated based on size, live cells, and expression of
551 CD4 or CD8 (depending on the experiment). DCs were incubated for 10 min on ice with the Fc
552 blocking antibody 2.4G2 prior to staining. DCs were gated based on size, live cells, and CD11c
553 expression. Mature DCs were further gated based on high expression of MHC-II, CD86 or CD80.

554 **T cell activation on stimulatory gel surfaces**

555 96 well plates coated with polyacrylamide hydrogels spanning a stiffness range of 2 – 25 kPa
556 were obtained from Matrigen. Hydrogel stiffness was verified by AFM at different locations
557 around the hydrogel surface (Figure 3 - Figure Supplement 1). Surfaces were first coated with 10
558 µg/ml of NeutrAvidin (ThermoFisher) and 2 µg/ml anti-CD28 (clone PV1) overnight at 4°C.
559 Primary amines in the NeutrAvidin form covalent bonds with quinone functional groups within
560 the hydrogels. The gel pore size is on the order of tens of nanometers, such that cells can only
561 interact with ligands bound on the gel surface. Surfaces were then washed twice with 200 µL of
562 PBS and coated with varying concentrations of biotinylated pMHC monomers (NIH tetramer
563 core facility) for 2 hours at 37°C. In cases where antibody stimulation was compared to pMHC
564 stimulation, surfaces were coated with varying concentrations of either biotinylated anti-CD3ε
565 (clone 2C11), or biotinylated anti-TCRvβ5.1/5.2 (clone MR9-4). In experiments where only
566 antibody stimulation was used, surfaces were coated directly with varying concentrations of
567 anti-CD3ε (clone 2C11) together with 2 µg/ml anti-CD28 (clone PV1) for 2 hours at 37°C.
568 Following coating, surfaces were washed 2 times with 200 µL of PBS, and blocked for 10 min
569 with T cell media containing 10% FBS prior to addition of 2.0×10^5 cells/well. Control studies
570 showed that stimulatory ligands bound slightly less well to stiffer hydrogel surfaces (Figure 3 -
571 Figure Supplement 2). Stiffer surfaces show the same or higher activating properties across all
572 assays, ruling out the possibility that differences in T cell activation are due to differential ligand
573 binding. Importantly, initial experiments included a 1 kPa hydrogel surface that yielded no

574 response across all assays. Therefore, data from this condition is not shown and was not
575 included in repeated experiments. For experiments where exogenous IL-2 was added, media
576 was supplemented with IL-2 to a final concentration of 25 U/ml. For measurements of
577 CD69/CD25 expression and IL-2 production, cells were harvested 22-24 hours post stimulation
578 for flow cytometry, and supernatants were used to measure IL-2 concentration using a mouse
579 IL-2 ELISA kit (Invitrogen). For early activation marker expression assays, cells were plated
580 immediately after isolation, and harvested 22-24 hours post stimulation for flow cytometry
581 analysis. For CFSE dilution assays, purified cells were washed once with PBS and stained for 3
582 min with 2.5 μ M CFSE (ThermoFisher). After quenching the excess CFSE by addition of 1 ml FBS
583 for 30 seconds, cells were washed and plated. Cells were harvested 44-48 hours (CD8 $^{+}$ T cells) or
584 68-72 hours (CD4 $^{+}$ T cells) post stimulation for flow cytometry analysis. For ligand comparison
585 assays, surfaces were first coated with 10 μ g/ml of NeutrAvidin (ThermoFisher) and 2 μ g/ml
586 anti-CD28 (PV1) overnight at 4°C. Surfaces were then washed twice with 200 μ L of PBS and
587 coated with varying concentrations of biotinylated ligands (anti-TCRV β 5.1/5.2, anti-CD3 ϵ , or
588 pMHC-II monomers) for 2 hours at 37°C.

589 **Cytotoxic T cell degranulation assays**

590 Assays were conducted on day 8 or 9 of culture. 2x10 5 CTLs were plated onto surfaces coated
591 with various concentrations of pMHC-I in the presence of 2 μ g/ml PE-conjugated anti-CD107a.
592 After 3 hours of re-stimulation, CD107a labeling was quantified by flow cytometry analysis. Cells
593 were gated based on size, live cells, and expression of CD8 $^{+}$. CD107a mean fluorescence
594 intensity (MFI) was extracted using FlowJo.

595 **Hydrogel ligand binding assays**

596 Hydrogel surfaces were coated with 1 μ g/ml pMHC-II monomers as described above. Hydrogel
597 wells were washed 3 times with 200 μ L of PBS and blocked for 1 hour with 0.25% bovine gelatin

598 in PBS solution. Following blocking, pMHC-II molecules were stained with 10 µg/ml rat anti
599 mouse I-A/I-E antibody (Clone M5/114) in 0.25% bovine gelatin in PBS solution for 1 hour at
600 room temperature. Wells were then washed 3 times and stained with Alexa 680 conjugated
601 goat anti rat secondary antibody diluted 1:500 in 0.25% Bovine gelatin in PBS solution for 1 hour
602 at room temperature. Finally, wells were washed and imaged using a Licor Odyssey CLx reader.

603

604 **T cell priming assays**

605 Priming assays were carried out in round bottom 96 well plates. 5×10^4 LPS-matured BMDCs
606 were plated in each well and pulsed with OVA₃₂₃₋₃₃₉ peptide at various concentrations (0.1 – 1
607 µg/ml). 1.5×10^5 CFSE stained, OT-II CD4⁺ T cells were added to each well and incubated for 68-72
608 hours. Cells were then harvested and analyzed using flow cytometry.

609 **Atomic force microscopy (AFM)**

610 All experiments were carried out at room temperature using a Bruker Bioscope Catalyst AFM
611 mounted on a Nikon TE200 inverted microscope. Micro-indentation measurements were made
612 with a spherical tip from Novascan. The tip was comprised of a 1 µm silicon dioxide particle
613 mounted on a silicon nitride cantilever with a nominal spring constant of 0.06 N/m; each
614 cantilever was calibrated using the thermal fluctuation method. The AFM was operated in fluid
615 contact mode, with 2 Hz acquisition. Total vertical cantilever displacement was set to 5 µm,
616 producing a maximal approach/retraction speed of ~20 µm/sec. Maximal deflection (Trigger
617 threshold) was adjusted for each cantilever to apply a maximal force of 6 nN on the measured
618 cell (e.g. for a 0.06 N/m cantilever, the trigger threshold was set to 100 nm). The actual
619 indentation depth was ~1.5 µm depending on the measured cell stiffness (Figure 1 –
620 Supplement Figure 4A,B). Analysis of force-distance curves was carried out using the Nanoscope
621 Analysis software (Bruker). The Young's modulus was extracted using the Hertzian model for

622 spherical tips with a contact point-based fitting on the extend curve data. Importantly, one of
623 the Hertzian model requirements is that indentation depth does not exceed the radius of the
624 spherical tip. Since the Bruker software we use does not allow one to restrict the fitting
625 algorithm based on Z axis displacement, we were unable to restrict fitting to exactly 0.5 μm .
626 Instead, we restricted the Hertzian model fitting to 30% of total force applied, which we found
627 corresponds to \sim 0.5 μm indentation depth (Figure 1 – Supplement Figure 4C). For each
628 individual cell, two separate measurements were conducted at different locations near, but not
629 directly over the nucleus. The reported cell stiffness value represents the average between
630 these independent measurements. Note that when measurements of cortical stiffness were
631 made over the nucleus, no significant differences in Young's modulus values were found (not
632 shown). To measure BMDC stiffness, 1×10^5 cells (untreated or LPS matured) were seeded onto
633 Poly L-lysine coated coverslips and allowed to spread for 4 hours at 37°C, 5% CO₂. Prior to data
634 acquisition, cells were incubated for 10 min with the Fc blocking antibody 2.4G2, washed and
635 stained for CD86 for 20 min, then washed and mounted on the AFM. All antibody incubations
636 and data acquisition steps were performed in L-15 media (Gibco) supplemented with 2mg/ml
637 glucose. For treated cell measurements, drugs [Latrunculin-B (10 μM), Cytochalasin-D (10 μM),
638 s-nitro-Blebbistatin (50 μM), Y27632 (25 μM), CK666 (100 μM), or SMIFH2 (10 μM)] were pre-
639 incubated with the cells at 37°C, 5% CO₂ for 30 min prior to Fc blocking and maintained in the
640 cultures throughout staining and data acquisition. Measured cells were visually selected based
641 on fluorescence; immature/mature cells were distinguished based on CD86 staining. In
642 experiments where the GFP-CA-WASp construct was expressed, GFP positive cells were selected
643 in conjunction with CD86 staining using a dual-band fluorescence filter set.

644 **Dendritic Cell Imaging**

645 1×10^5 DCs (untreated or LPS matured) either from WT or GFP-Lifeact Tg mice, were seeded onto
646 Poly L-lysine coated hydrogels or glass coverslips and allowed to spread for 4 hours at 37°C, 5%
647 CO₂. Prior to imaging, cells were incubated for 10 min with the Fc blocking antibody 2.4G2,
648 washed and stained with Alexa647 conjugated anti-CD86 (Clone GL-1) for 20 min, then washed
649 and mounted on the microscope. Antibody incubations and data acquisition steps were
650 performed in L-15 media (Gibco) supplemented with 2mg/ml glucose. Imaging DCs on hydrogels
651 was done using a 40X, long working distance objective through the hydrogels.

652 **Statistical Methods**

653 All datasets were subjected to outlier analysis prior to execution of statistical testing. Outliers
654 were defined as data points with values outside the range of mean +/- 2.5xStDev, and were
655 deleted from the dataset. Testing for a statistically significant difference between experimental
656 groups was done using an unpaired one-way ANOVA test with a post-hoc Tukey correction for
657 multiple comparisons.

658 Throughout the paper, data shown represents biological, and not technical, replicates. For
659 BMDC assays, a single experiment constitutes measurement of multiple cells from a fresh DC
660 culture, starting from frozen or freshly harvested bone marrow. For splenic DCs, a single
661 experiment constitutes measurement of multiple cells freshly purified from the spleen of a
662 single mouse. In each experiment, WT or untreated cells were measured side by side with
663 treated cells as a standard control. For T cell assays, a single experiment constitutes cells freshly
664 purified from spleen and lymph nodes of a single animal. All CFSE dilution assays were executed
665 in technical duplicates, although a single data set is presented. When needed, figure legends
666 describe the quantity of technical repeats used in an experiment.

667 **ACKNOWLEDGEMENTS**

668 The authors thank Florin Tuluc and Jennifer Murray from the Children's Hospital of Philadelphia
669 Flow Cytometry core. We thank the biomechanics core of the Institute of Translational Medicine
670 and Therapeutics (ITMAT) at the University of Pennsylvania for use of the Atomic Force
671 Microscope and the NIH tetramer core facility for provision of MHC-peptide complexes. We
672 thank Dr. Shuixing Li and Dr. Nathan Roy for expert technical assistance, Dr. Nathan Roy and Mr.
673 Tanner Robertson for critical reading of the manuscript, and members of the Burkhardt
674 laboratory for many helpful discussions. This work was supported by NIH grants R01 GM104867
675 and R21 AI32828 to JKB.

676 **ETHICS STATEMENT**

677 All studies, breeding and maintenance of animals was performed under Animal Care and Use
678 Protocol #667, as approved by The Children's Hospital of Philadelphia Institutional Animal Care
679 and Use Committee.

680 **FIGURE LEGENDS**681 **Figure 1. DC maturation induces an actin-dependent increase in cortical stiffness.**

682 (A) BMDCs were untreated or matured by treatment with LPS, and cortical stiffness was
683 measured by AFM micro-indentation. Fluorescent anti-CD86 labeling was used to select
684 immature (CD86-negative) or mature (CD86 high) cells. (B) Ex-vivo DCs were purified from
685 spleens of untreated mice or from mice injected with LPS 24 hours prior to harvesting the
686 spleen, and analyzed as in A. (C) Immature or LPS matured BMDCs either left untreated or
687 treated with 10 μ m of the actin de-polymerizing agents Latrunculin-B or Cytochalasin-D prior to
688 AFM measurements. (D) Immature or LPS matured BMDCs were plated on substrates of
689 different stiffness prior to AFM measurements. Data are pooled from 2-3 independent
690 experiments. Each data point represents an average of two stiffness measurements at different
691 locations around a single cell nucleus. Error bars denote standard deviation. n.s non-significant,
692 **p<0.01, ****p<0.0001 calculated by an unpaired one-way ANOVA, post-hoc Tukey corrected
693 test.

694 **Figure 2. Effects of actin regulatory proteins on DC cortical stiffness.**

695 Murine BMDCs from WT mice or mice lacking key actin-associated proteins were untreated or
696 matured by treatment with LPS, and cortical stiffness was measured by AFM micro-indentation.
697 To facilitate comparison between experiments, results were normalized to values of mature WT
698 BMDCs in each experiment. (A) Cortical stiffness of BMDCs from mice lacking important actin
699 modulating proteins. (B) Cortical stiffness of WT BMDCs treated with cytoskeletal inhibitors.
700 CK666 (100 μ M) was used to inhibit branched actin polymerization by Arp2/3. SMIFH2 (10 μ m)
701 was used to inhibit linear actin polymerization by formins. Acto-myosin contractility was
702 inhibited directly with Blebbistatin (50 μ M) or indirectly with the Rho-kinase inhibitor Y27623 (25
703 μ M). All drugs had no effect on immature BMDCs (data not shown). Data points for untreated

704 WT BMDCs (both immature and mature) were pooled from all experiments as a reference. The
705 dashed line represents the average stiffness of untreated mature WT BMDCs from all
706 experiments. Data are pooled from 2-3 independent experiments. Each data point represents an
707 average of two stiffness measurements at different locations around a single cell nucleus. Error
708 bars denote standard deviation. n.s non-significant, *p<0.05, **p<0.01, ***p<0.001,
709 ****p<0.0001 calculated by an unpaired one-way ANOVA, with post-hoc Tukey correction.

710 **Figure 3. CD4⁺ and CD8⁺ T cells demonstrate vastly different stiffness responses.**

711 Murine T cells were purified from lymph nodes and spleen and activated on stimulatory
712 acrylamide hydrogel surfaces with a stiffness range of 2 – 25 kPa and plastic (PL). Stimulatory
713 surfaces were coated with the indicated concentrations of pMHC-I or pMHC-II together with 2
714 µg/ml anti-CD28 to stimulate OT-I CD8⁺ or OTI-II CD4⁺ T cells, respectively. (A,B,D,E) Cells were
715 harvested 24 hours post activation and expression of early activation markers was measured by
716 flow cytometry. Data represent averages +/- SEM of percent positive cells from N=3
717 independent experiments. (A,B) CD4⁺ T cells show profound stiffness dependent expression of
718 both markers. (C,F) Cell supernatants were collected at 24 hours and IL-2 expression was
719 analyzed by ELISA. Data represent means +/- StDev from 3-6 replicate samples from one
720 representative experiment, N=2 experiments.

721 **Figure 4. CD4 T cell proliferation is stiffness dependent and IL-2 independent.**

722 OT-II CD4⁺ T cells were purified from lymph nodes and spleen and activated on stimulatory
723 acrylamide hydrogel surfaces with a stiffness range of 2 – 25 kPa and plastic (PL). Stimulatory
724 surfaces were coated with the indicated concentrations of pMHC-II together with 2 µg/ml anti-
725 CD28. (A,B) Proliferation of CD4⁺ T cells was measured by CFSE dilution at 72 hours post
726 activation, showing profound stiffness-dependent proliferation. (A) Representative CFSE dilution
727 matrix from a single experiment. (B) Average division index from 3 independent experiments. (C)

728 Representative plots of CD25 expression as a function of CFSE dilution at 72 hours from a single
729 experiment shows that upregulation of CD25 on T cell membrane precedes proliferation. (D)
730 Average percent of T cells expressing CD25 from 3 independent experiments. (E) Division index
731 of CD4⁺ T cells activated with or without addition of 25 U/ml of exogenous IL-2. Data in B, D, and
732 E represent averages +/- SEM from at least 3 independent experiments.

733 **Figure 5. CD8⁺ T cell proliferation and degranulation show moderate stiffness dependency**

734 Naïve OT-I CD8⁺ T cells were purified from lymph nodes and spleen and activated on stimulatory
735 acrylamide hydrogel surfaces with a stiffness range of 2 – 25 kPa and plastic (PL). Stimulatory
736 surfaces were coated with the indicated concentrations of pMHC-I together with 2 µg/ml anti-
737 CD28 (A,B) Proliferation of CD8⁺ T cells was measured by CFSE dilution at 72 hours post
738 activation, showing only moderate stiffness-dependent proliferation. (A) Representative CFSE
739 dilution matrix from a single experiment. Note that the threshold pMHC-I concentration needed
740 to induce proliferation is very similar between the different stiffness surfaces. (B) Average
741 division index from 3 independent experiments. (C) representative plot of CD25 expression as a
742 function of CFSE dilution at 72 hours from a single experiment shows a binary stiffness response.
743 Note that with low doses of pMHC-I, only cells stimulated on very stiff substrates (25kPa or
744 plastic) survived and proliferated. Percent of live cells is given for each condition. (D) Average
745 percent of T cells expressing CD25 from 2 independent experiments. Levels of CD25 membrane
746 expression are very similar between the different substrates, probably reflecting the fact that
747 only T cells that upregulate CD25 survive. (E) Cytotoxic CD8⁺ T cells on days 8 or 9 of culture
748 were restimulated on hydrogel surfaces with a range of pMHC-I concentrations, and
749 degranulation was measured based on surface exposure of CD107a (N=3). Data in B, D, and E
750 represent averages +/- SEM from at least 3 independent experiments.

751

752 **Figure 6. Stimulation of TCR with pMHC leads to the strongest stiffness-dependent response.**
753 OT-II CD4⁺ T cells were stimulated on acrylamide hydrogels of different stiffnesses coated with
754 the indicated range of stimulatory ligands. Proliferation and membrane expression of CD25 were
755 measured 72 hours post activation by flow cytometry. (A,D) Stimulation with anti-CD3ε
756 antibody. (B,E) Stimulation with anti-TCRβ antibody. (C,F) Stimulation with pMHC-II. Plots show
757 the average division index or CD25 expression from 3 independent experiment. Gray areas
758 denote a similar range of stimulatory ligand molar concentrations to aid comparison.

759 **Figure 7. DC cortical stiffness acts as a costimulatory signal for T cell activation**
760 WT or WASp^{-/-} BMDCs, or WT BMDCs transduced with constitutively active form of WASp (CA-
761 WASp) were untreated or matured by treatment with LPS. (A) Cortical stiffness was measured
762 by AFM micro-indentation. Each data point represents an average of two stiffness
763 measurements at different locations around a single cell nucleus. Error bars denote standard
764 deviation. ***p<0.001, ****p<0.0001 calculated by an unpaired one-way ANOVA, comparing
765 mature WT with all other treatments, with post-hoc Tukey correction. (B,C) LPS-matured BMDCs
766 were pulsed with a range of OVA₃₂₃₋₃₃₉ peptide concentrations and co-cultured with *ex-vivo* OT-II
767 CD4⁺ T cells for 72 hrs. Proliferation was measured by CFSE dilution. (D,E) Proliferation index
768 pooled from two independent experiments. (F-G) Division index values pooled from two
769 independent experiments. Error bars represent StDev.

770 **Figure 1 – Figure Supplement 1. Selecting mature or immature BMDCs based on CD86 staining.**
771 40X images of LPS treated BMDCs stained with Alexa 488-αCD86, demonstrating how cells were
772 selected for AFM measurements. Images clearly show that while many cells express high levels
773 of CD86, some express little to none. Only cells expressing high levels of CD86 (yellow arrows)
774 were selected for analysis of mature BMDCs.

775 **Figure 1 – Figure Supplement 2. Analysis of BMDC spreading on hydrogel and glass surfaces.**
776 BMDCs were allowed to spread for 4 hours on 2kPa and 25kPa hydrogels or glass surfaces. Cells
777 were imaged through the hydrogel using a 40X, long working distance objective. (A,C)
778 Representative phase contrast images of mature and immature BMDC. (B,D) Analysis of
779 spreading area, determined from parallel widefield fluorescence images of cells expressing GFP-
780 Lifeact.

781 **Figure 1 – Figure Supplement 3. Validation of hydrogel compliances.**
782 Direct AFM measurements of hydrogel compliance, validating the stiffness of hydrogels used for
783 measuring the effects of substrate compliance on DC stiffness

784 **Figure 1 – Figure Supplement 4. Indentation length and Hertzian model fitting on AFM data**
785 Indentation length was defined as the distance between initial deflection to maximal cantilever
786 displacement. (A) An example of a force curve and the extraction of the *de-facto* indentation
787 length. (B) Quantification of indentation length for immature and mature DCs. (C) Example of
788 fitting the data with the Hertzian model to calculate the Young's modulus. Fitting is restricted to
789 30% of total force applied, which corresponds to ~0.5 μ m indentation depth. Note that the
790 contact point set by the fitting algorithm differs from the reference point used for the
791 indentation length calculation (compare the dashed black line with the rightmost dashed green
792 line).

793 **Figure 3 – Figure Supplement 1. Validation of hydrogel compliances.**
794 Direct AFM measurements of hydrogel compliance, validating the stiffness of hydrogel surfaces
795 used for activation of T-cells.

796 **Figure 3 - Figure Supplement 2. Binding of pMHC complex to various hydrogel surfaces**
797 Hydrogel surfaces were coated with 1 μ g/ml pMHC-II complex, blocked with 0.25% Bovine

798 gelatin, then stained with rat-anti-mouse I-A\I-E followed by goat-anti-Rat Alexa680. (A)
799 Fluorescence image of uncoated, unstained and stained hydrogels using a LI-COR Odyssey
800 reader. (B) Quantification of mean fluorescence intensity for the center of each well. Each data
801 point represents a single hydrogel well (all measurements were made in duplicate); lines show
802 mean values. Similar results were obtained using fluorescent neutravidin (not shown).

803 **Figure 5 - Figure Supplement 1. Comparing T cell activation with 2C11 and pMHC complexes**
804 Comparison of T cells activated on surfaces coated with a constant dose of α CD28 together with
805 varying concentrations with 2C11 or pMHC complexes. Division indices were normalized within
806 each dataset to facilitate comparison of stiffness responses. (A,B) OT-II CD4 T cells stimulated
807 with (A) 2C11 (N=3) or (B) pMHC-II (normalized data from Figure 4B, N=3). Note that regardless
808 of whether CD4 $^{+}$ T cells are stimulated with 2C11 or pMHC, they show they show a large
809 increase in proliferation between 4 and 8kPa. (C,D) OT-I CD8 T cells activated on varying
810 concentrations of (C) 2C11 (N=3) or (D) pMHC-II (normalized data from figure 5B, N=3). In both
811 cases, only modest stiffness responses are observed.

812

814 References

- 815 Al-Alwan, M. M., Rowden, G., Lee, T. D., & West, K. A. (2001). The dendritic cell cytoskeleton is
 816 critical for the formation of the immunological synapse. *J Immunol*, 166(3), 1452-1456.
- 817 Alatoom, A., Sapudom, J., Soni, P., Mohamed, W. K. E., Garcia-Sabate, A., & Teo, J. (2020).
 818 Artificial Biosystem for Modulation of Interactions between Antigen-Presenting Cells
 819 and T Cells. *Adv Biosyst*, n/a(n/a), e2000039. doi:10.1002/adbi.202000039
- 820 Barnden, M. J., Allison, J., Heath, W. R., & Carbone, F. R. (1998). Defective TCR expression in
 821 transgenic mice constructed using cDNA-based alpha- and beta-chain genes under the
 822 control of heterologous regulatory elements. *Immunology and Cell Biology*, 76(1), 34-40.
 823 doi:10.1046/j.1440-1711.1998.00709.x
- 824 Bashour, K. T., Gondarenko, A., Chen, H., Shen, K., Liu, X., Huse, M., . . . Kam, L. C. (2014). CD28
 825 and CD3 have complementary roles in T-cell traction forces. *Proc Natl Acad Sci U S A*,
 826 111(6), 2241-2246. doi:10.1073/pnas.1315606111
- 827 Basu, R., Whitlock, B. M., Husson, J., Le Floc'h, A., Jin, W., Oyler-Yaniv, A., . . . Huse, M. (2016).
 828 Cytotoxic T Cells Use Mechanical Force to Potentiate Target Cell Killing. *Cell*, 165(1), 100-
 829 110. doi:10.1016/j.cell.2016.01.021
- 830 Beel, K., Cotter, M. M., Blatny, J., Bond, J., Lucas, G., Greene, F., . . . Vandenbergh, P. (2009). A
 831 LARGE KINDRED WITH X-LINKED NEUTROPENIA WITH AN I294T MUTATION OF THE
 832 WISKOTT-ALDRICH SYNDROME GENE. *British journal of haematology*, 144(1), 120-126.
 833 doi:10.1111/j.1365-2141.2008.07416.x
- 834 Blumenthal, D., & Burkhardt, J. K. (2020). Multiple actin networks coordinate
 835 mechanotransduction at the immunological synapse. *J Cell Biol*, 219(2).
 836 doi:10.1083/jcb.201911058
- 837 Bouma, G., Burns, S., & Thrasher, A. J. (2007). Impaired T-cell priming in vivo resulting from
 838 dysfunction of WASp-deficient dendritic cells. *Blood*, 110(13), 4278-4284.
 839 doi:10.1182/blood-2007-06-096875
- 840 Bouma, G., Mendoza-Naranjo, A., Blundell, M. P., de Falco, E., Parsley, K. L., Burns, S. O., &
 841 Thrasher, A. J. (2011). Cytoskeletal remodeling mediated by WASp in dendritic cells is
 842 necessary for normal immune synapse formation and T-cell priming. *Blood*, 118(9),
 843 2492-2501. doi:10.1182/blood-2011-03-340265
- 844 Bufl, N., Saitakis, M., Dogniaux, S., Buschinger, O., Bohineust, A., Richert, A., . . . Asnacios, A.
 845 (2015). Human Primary Immune Cells Exhibit Distinct Mechanical Properties that Are
 846 Modified by Inflammation. *Biophysical Journal*, 108(9), 2181-2190.
 847 doi:10.1016/j.bpj.2015.03.047
- 848 Burns, S., Hardy, S. J., Buddle, J., Yong, K. L., Jones, G. E., & Thrasher, A. J. (2004). Maturation of
 849 DC is associated with changes in motile characteristics and adherence. *Cell Motil
 850 Cytoskeleton*, 57(2), 118-132. doi:10.1002/cm.10163
- 851 Burns, S., Thrasher, A. J., Blundell, M. P., Machesky, L., & Jones, G. E. (2001). Configuration of
 852 human dendritic cell cytoskeleton by Rho GTPases, the WAS protein, and differentiation.
 853 *Blood*, 98(4), 1142-1149.
- 854 Byfield, F. J., Reen, R. K., Shentu, T. P., Levitan, I., & Gooch, K. J. (2009). Endothelial actin and cell
 855 stiffness is modulated by substrate stiffness in 2D and 3D. *J Biomech*, 42(8), 1114-1119.
 856 doi:10.1016/j.jbiomech.2009.02.012

- 857 Calle, Y., Chou, H. C., Thrasher, A. J., & Jones, G. E. (2004). Wiskott-Aldrich syndrome protein and
858 the cytoskeletal dynamics of dendritic cells. *Journal of Pathology*, 204(4), 460-469.
859 doi:10.1002/path.1651
- 860 Comrie, W. A., Li, S., Boyle, S., & Burkhardt, J. K. (2015). The dendritic cell cytoskeleton promotes
861 T cell adhesion and activation by constraining ICAM-1 mobility. *J Cell Biol*, 208(4), 457-
862 473. doi:10.1083/jcb.201406120
- 863 Das, D. K., Feng, Y., Mallis, R. J., Li, X., Keskin, D. B., Hussey, R. E., . . . Lang, M. J. (2015). Force-
864 dependent transition in the T-cell receptor beta-subunit allosterically regulates peptide
865 discrimination and pMHC bond lifetime. *Proc Natl Acad Sci U S A*, 112(5), 1517-1522.
866 doi:10.1073/pnas.1424829112
- 867 Demoulin, D., Carlier, M. F., Bibette, J., & Baudry, J. (2014). Power transduction of actin
868 filaments ratcheting in vitro against a load. *Proc Natl Acad Sci U S A*, 111(50), 17845-
869 17850. doi:10.1073/pnas.1414184111
- 870 Discher, D. E., Janmey, P., & Wang, Y.-I. (2005). Tissue Cells Feel and Respond to the Stiffness of
871 Their Substrate. *Science*, 310(5751), 1139-1143. doi:10.1126/science.1116995
- 872 Doan, T., McNally, A., Thomas, R., & Steptoe, R. J. (2009). Steady-state dendritic cells
873 continuously inactivate T cells that escape thymic negative selection. *Immunol Cell Biol*,
874 87(8), 615-622. doi:10.1038/icb.2009.46
- 875 Dustin, M. L. (2014). The immunological synapse. *Cancer Immunol Res*, 2(11), 1023-1033.
876 doi:10.1158/2326-6066.CIR-14-0161
- 877 Engler, A. J., Sen, S., Sweeney, H. L., & Discher, D. E. Matrix Elasticity Directs Stem Cell Lineage
878 Specification. *Cell*, 126(4), 677-689. doi:10.1016/j.cell.2006.06.044
- 879 Fisher, P. J., Bulur, P. A., Vuk-Pavlovic, S., Prendergast, F. G., & Dietz, A. B. (2008). Dendritic cell
880 microvilli: a novel membrane structure associated with the multifocal synapse and T-cell
881 clustering. *Blood*, 112(13), 5037-5045. doi:10.1182/blood-2008-04-149526
- 882 Friedl, P., den Boer, A. T., & Gunzer, M. (2005). Tuning immune responses: diversity and
883 adaptation of the immunological synapse. *Nat Rev Immunol*, 5(7), 532-545.
884 doi:10.1038/nri1647
- 885 Garrett, W. S., Chen, L. M., Kroschewski, R., Ebersold, M., Turley, S., Trombetta, S., . . . Mellman,
886 I. (2000). Developmental control of endocytosis in dendritic cells by Cdc42. *Cell*, 102(3),
887 325-334.
- 888 Gleisner, M. A., Rosemblatt, M., Fierro, J. A., & Bono, M. R. (2011). Delivery of alloantigens via
889 apoptotic cells generates dendritic cells with an immature tolerogenic phenotype.
890 *Transplant Proc*, 43(6), 2325-2333. doi:10.1016/j.transproceed.2011.06.007
- 891 Gordon, J. R., Ma, Y., Churchman, L., Gordon, S. A., & Dawicki, W. (2014). Regulatory dendritic
892 cells for immunotherapy in immunologic diseases. *Front Immunol*, 5, 7.
893 doi:10.3389/fimmu.2014.00007
- 894 Guilliams, M., & Malissen, B. (2015). A Death Notice for In-Vitro-Generated GM-CSF Dendritic
895 Cells? *Immunity*, 42(6), 988-990. doi:10.1016/j.jimmuni.2015.05.020
- 896 Harding, F. A., McArthur, J. G., Gross, J. A., Raulet, D. H., & Allison, J. P. (1992). CD28-mediated
897 signalling co-stimulates murine T cells and prevents induction of anergy in T-cell clones.
898 *Nature*, 356(6370), 607-609. doi:10.1038/356607a0
- 899 Hogquist, K. A., Jameson, S. C., Heath, W. R., Howard, J. L., Bevan, M. J., & Carbone, F. R. (1994).
900 T cell receptor antagonist peptides induce positive selection. *Cell*, 76(1), 17-27.
901 doi:10.1016/0092-8674(94)90169-4
- 902 Hong, J., Persaud, S. P., Horvath, S., Allen, P. M., Evavold, B. D., & Zhu, C. (2015). Force-
903 Regulated In Situ TCR-Peptide-Bound MHC Class II Kinetics Determine Functions of CD4+
904 T Cells. *J Immunol*, 195(8), 3557-3564. doi:10.4049/jimmunol.1501407

- 905 Huang, Y., Biswas, C., Klos Dehring, D. A., Sriram, U., Williamson, E. K., Li, S., . . . Burkhardt, J. K.
906 (2011). The actin regulatory protein HS1 is required for antigen uptake and presentation
907 by dendritic cells. *Journal of Immunology*, 187(11), 5952-5963.
908 doi:10.4049/jimmunol.1100870
- 909 Hui, K. L., Balagopalan, L., Samelson, L. E., & Upadhyaya, A. (2015). Cytoskeletal forces during
910 signaling activation in Jurkat T-cells. *Mol Biol Cell*, 26(4), 685-695. doi:10.1091/mbc.E14-
911 03-0830
- 912 Husson, J., Chemin, K., Bohineust, A., Hivroz, C., & Henry, N. (2011). Force generation upon T cell
913 receptor engagement. *PLoS One*, 6(5), e19680. doi:10.1371/journal.pone.0019680
- 914 Inaba, K., Inaba, M., Romani, N., Aya, H., Deguchi, M., Ikehara, S., . . . Steinman, R. M. (1992).
915 Generation of large numbers of dendritic cells from mouse bone marrow cultures
916 supplemented with granulocyte/macrophage colony-stimulating factor. *The Journal of
917 Experimental Medicine*, 176(6), 1693-1702. doi:10.1084/jem.176.6.1693
- 918 Judokusumo, E., Tabdanov, E., Kumari, S., Dustin, M. L., & Kam, L. C. (2012). Mechanosensing in
919 T lymphocyte activation. *Biophysical Journal*, 102(2), L5-7.
920 doi:10.1016/j.bpj.2011.12.011
- 921 Jung, S., Unutmaz, D., Wong, P., Sano, G., De los Santos, K., Sparwasser, T., . . . Lang, R. A. (2002).
922 In vivo depletion of CD11c+ dendritic cells abrogates priming of CD8+ T cells by
923 exogenous cell-associated antigens. *Immunity*, 17(2), 211-220.
- 924 Kim, S. T., Takeuchi, K., Sun, Z. Y., Touma, M., Castro, C. E., Fahmy, A., . . . Reinherz, E. L. (2009).
925 The alphabeta T cell receptor is an anisotropic mechanosensor. *J Biol Chem*, 284(45),
926 31028-31037. doi:10.1074/jbc.M109.052712
- 927 Knight, S. C., Farrant, J., Bryant, A., Edwards, A. J., Burman, S., Lever, A., . . . Webster, A. D.
928 (1986). Non-adherent, low-density cells from human peripheral blood contain dendritic
929 cells and monocytes, both with veiled morphology. *Immunology*, 57(4), 595-603.
- 930 Lahm, H. W., & Stein, S. (1985). Characterization of recombinant human interleukin-2 with
931 micromethods. *J Chromatogr*, 326, 357-361.
- 932 Lee, M. S., Glassman, C. R., Deshpande, N. R., Badgandi, H. B., Parrish, H. L., Uttamapinant, C., . . .
933 Kuhns, M. S. (2015). A Mechanical Switch Couples T Cell Receptor Triggering to the
934 Cytoplasmic Juxtamembrane Regions of CD3zetazeta. *Immunity*, 43(2), 227-239.
935 doi:10.1016/j.jimmuni.2015.06.018
- 936 Levitsky, H. I., Montgomery, J., Ahmadzadeh, M., Staveley-O'Carroll, K., Guarnieri, F., Longo, D.
937 L., & Kwak, L. W. (1996). Immunization with granulocyte-macrophage colony-stimulating
938 factor-transduced, but not B7-1-transduced, lymphoma cells primes idiotype-specific T
939 cells and generates potent systemic antitumor immunity. *J Immunol*, 156(10), 3858-
940 3865.
- 941 Li, Y. C., Chen, B. M., Wu, P. C., Cheng, T. L., Kao, L. S., Tao, M. H., . . . Roffler, S. R. (2010). Cutting
942 Edge: mechanical forces acting on T cells immobilized via the TCR complex can trigger
943 TCR signaling. *J Immunol*, 184(11), 5959-5963. doi:10.4049/jimmunol.0900775
- 944 Liu, B., Chen, W., Evavold, B. D., & Zhu, C. (2014). Accumulation of dynamic catch bonds
945 between TCR and agonist peptide-MHC triggers T cell signaling. *Cell*, 157(2), 357-368.
946 doi:10.1016/j.cell.2014.02.053
- 947 Lo, C.-M., Wang, H.-B., Dembo, M., & Wang, Y.-I. Cell Movement Is Guided by the Rigidity of the
948 Substrate. *Biophysical Journal*, 79(1), 144-152. doi:10.1016/S0006-3495(00)76279-5
- 949 Lutz, M. B., Inaba, K., Schuler, G., & Romani, N. (2016). Still Alive and Kicking: In-Vitro-Generated
950 GM-CSF Dendritic Cells! *Immunity*, 44(1), 1-2. doi:10.1016/j.jimmuni.2015.12.013
- 951 Ma, Z., Janmey, P. A., & Finkel, T. H. (2008). The receptor deformation model of TCR triggering.
952 *FASEB J*, 22(4), 1002-1008. doi:10.1096/fj.07-9331hyp

- 953 McAdam, A. J., Schweitzer, A. N., & Sharpe, A. H. (1998). The role of B7 co-stimulation in
954 activation and differentiation of CD4+ and CD8+ T cells. *Immunol Rev*, 165, 231-247.
955 doi:10.1111/j.1600-065x.1998.tb01242.x
- 956 Mellman, I., & Steinman, R. M. (2001). Dendritic cells: specialized and regulated antigen
957 processing machines. *Cell*, 106(3), 255-258.
- 958 Na, Y. R., Jung, D., Gu, G. J., & Seok, S. H. (2016). GM-CSF Grown Bone Marrow Derived Cells Are
959 Composed of Phenotypically Different Dendritic Cells and Macrophages. *Mol Cells*,
960 39(10), 734-741. doi:10.14348/molcells.2016.0160
- 961 O'Connor, R. S., Hao, X., Shen, K., Bashour, K., Akimova, T., Hancock, W. W., . . . Milone, M. C.
962 (2012). Substrate rigidity regulates human T cell activation and proliferation. *Journal of
963 Immunology*, 189(3), 1330-1339. doi:10.4049/jimmunol.1102757
- 964 Oakes, P. W., Patel, D. C., Morin, N. A., Zitterbart, D. P., Fabry, B., Reichner, J. S., & Tang, J. X.
965 (2009). Neutrophil morphology and migration are affected by substrate elasticity. *Blood*,
966 114(7), 1387-1395. doi:10.1182/blood-2008-11-191445
- 967 Pelham, R. J., & Wang, Y.-I. (1997). Cell locomotion and focal adhesions are regulated by
968 substrate flexibility. *Proceedings of the National Academy of Sciences*, 94(25), 13661-
969 13665.
- 970 Pryshchep, S., Zarnitsyna, V. I., Hong, J., Evavold, B. D., & Zhu, C. (2014). Accumulation of serial
971 forces on TCR and CD8 frequently applied by agonist antigenic peptides embedded in
972 MHC molecules triggers calcium in T cells. *J Immunol*, 193(1), 68-76.
973 doi:10.4049/jimmunol.1303436
- 974 Renkawitz, J., Schumann, K., Weber, M., Lammermann, T., Pflicke, H., Piel, M., . . . Sixt, M.
975 (2009). Adaptive force transmission in amoeboid cell migration. *Nat Cell Biol*, 11(12),
976 1438-1443. doi:10.1038/ncb1992
- 977 Saitakis, M., Dogniaux, S., Goudot, C., Bufl, N., Asnacios, S., Maurin, M., . . . Hivroz, C. (2017).
978 Different TCR-induced T lymphocyte responses are potentiated by stiffness with variable
979 sensitivity. *eLife*, 6. doi:10.7554/eLife.23190
- 980 Salbreux, G., Charras, G., & Paluch, E. (2012). Actin cortex mechanics and cellular
981 morphogenesis. *Trends Cell Biol*, 22(10), 536-545. doi:10.1016/j.tcb.2012.07.001
- 982 Sawicka, A., Babataheri, A., Dogniaux, S., Barakat, A. I., Gonzalez-Rodriguez, D., Hivroz, C., &
983 Husson, J. (2017). Micropipette force probe to quantify single-cell force generation:
984 application to T-cell activation. *Mol Biol Cell*, 28(23), 3229-3239. doi:10.1091/mbc.E17-
985 06-0385
- 986 Snapper, S. B., Rosen, F. S., Mizoguchi, E., Cohen, P., Khan, W., Liu, C. H., . . . Alt, F. W. (1998).
987 Wiskott-Aldrich syndrome protein-deficient mice reveal a role for WASP in T but not B
988 cell activation. *Immunity*, 9(1), 81-91.
- 989 Solon, J., Levental, I., Sengupta, K., Georges, P. C., & Janmey, P. A. Fibroblast Adaptation and
990 Stiffness Matching to Soft Elastic Substrates. *Biophysical Journal*, 93(12), 4453-4461.
991 doi:10.1529/biophysj.106.101386
- 992 Sun, Z. J., Kim, K. S., Wagner, G., & Reinherz, E. L. (2001). Mechanisms contributing to T cell
993 receptor signaling and assembly revealed by the solution structure of an ectodomain
994 fragment of the CD3 epsilon gamma heterodimer. *Cell*, 105(7), 913-923.
995 doi:10.1016/s0092-8674(01)00395-6
- 996 Swamy, M., Beck-Garcia, K., Beck-Garcia, E., Hartl, F. A., Morath, A., Yousefi, O. S., . . . Schamel,
997 W. W. (2016). A Cholesterol-Based Allostery Model of T Cell Receptor Phosphorylation.
998 *Immunity*, 44(5), 1091-1101. doi:10.1016/j.jimmuni.2016.04.011
- 999 Taniuchi, I., Kitamura, D., Maekawa, Y., Fukuda, T., Kishi, H., & Watanabe, T. (1995). Antigen-
1000 receptor induced clonal expansion and deletion of lymphocytes are impaired in mice

- 1001 lacking HS1 protein, a substrate of the antigen-receptor-coupled tyrosine kinases. *EMBO J*, 14(15), 3664-3678.
- 1002
- 1003 Tee, S. Y., Fu, J., Chen, C. S., & Janmey, P. A. (2011). Cell shape and substrate rigidity both
1004 regulate cell stiffness. *Biophys J*, 100(5), L25-27. doi:10.1016/j.bpj.2010.12.3744
- 1005 Tello-Lafoz, M., Srpan, K., Hu, J., Romin, Y., Calò, A., Hsu, K. C., . . . Er, E. E. (2020). Cytotoxic
1006 lymphocytes use mechanosurveillance to target biophysical vulnerabilities in cancer.
1007 *bioRxiv*, 2020.2004.2021.054304. doi:10.1101/2020.04.21.054304
- 1008 Trappmann, B., Gautrot, J. E., Connelly, J. T., Strange, D. G. T., Li, Y., Oyen, M. L., . . . Huck, W. T.
1009 S. (2012). Extracellular-matrix tethering regulates stem-cell fate. *Nature Materials*, 11,
1010 642. doi:10.1038/nmat3339
- 1011 van Helden, S. F., Oud, M. M., Joosten, B., Peterse, N., Figdor, C. G., & van Leeuwen, F. N. (2008).
1012 PGE2-mediated podosome loss in dendritic cells is dependent on actomyosin
1013 contraction downstream of the RhoA-Rho-kinase axis. *J Cell Sci*, 121(Pt 7), 1096-1106.
1014 doi:10.1242/jcs.020289
- 1015 Vargas, P., Maiuri, P., Bretou, M., Saez, P. J., Pierobon, P., Maurin, M., . . . Lennon-Dumenil, A.
1016 M. (2016). Innate control of actin nucleation determines two distinct migration
1017 behaviours in dendritic cells. *Nat Cell Biol*, 18(1), 43-53. doi:10.1038/ncb3284
- 1018 Verdijk, P., van Veelen, P. A., de Ru, A. H., Hensbergen, P. J., Mizuno, K., Koerten, H. K., . . .
1019 Mommaas, A. M. (2004). Morphological changes during dendritic cell maturation
1020 correlate with cofilin activation and translocation to the cell membrane. *Eur J Immunol*,
1021 34(1), 156-164. doi:10.1002/eji.200324241
- 1022 West, M. A., Prescott, A. R., Eskelinne, E. L., Ridley, A. J., & Watts, C. (2000). Rac is required for
1023 constitutive macropinocytosis by dendritic cells but does not control its downregulation.
1024 *Curr Biol*, 10(14), 839-848.
- 1025 Westerberg, L. S., Meelu, P., Baptista, M., Eston, M. A., Adamovich, D. A., Cotta-de-Almeida, V., .
1026 . . . Snapper, S. B. (2010). Activating WASP mutations associated with X-linked
1027 neutropenia result in enhanced actin polymerization, altered cytoskeletal responses,
1028 and genomic instability in lymphocytes. *The Journal of Experimental Medicine*, 207(6),
1029 1145-1152. doi:10.1084/jem.20091245
- 1030 Wu, P. H., Aroush, D. R., Asnacios, A., Chen, W. C., Dokukin, M. E., Doss, B. L., . . . Wirtz, D.
1031 (2018). A comparison of methods to assess cell mechanical properties. *Nat Methods*,
1032 15(7), 491-498. doi:10.1038/s41592-018-0015-1
- 1033 Xu, C., Gagnon, E., Call, M. E., Schnell, J. R., Schwieters, C. D., Carman, C. V., . . . Wucherpfennig,
1034 K. W. (2008). Regulation of T cell receptor activation by dynamic membrane binding of
1035 the CD3epsilon cytoplasmic tyrosine-based motif. *Cell*, 135(4), 702-713.
1036 doi:10.1016/j.cell.2008.09.044
- 1037 Yamashiro, S. (2012). Functions of fascin in dendritic cells. *Crit Rev Immunol*, 32(1), 11-21.
- 1038

Figure 1

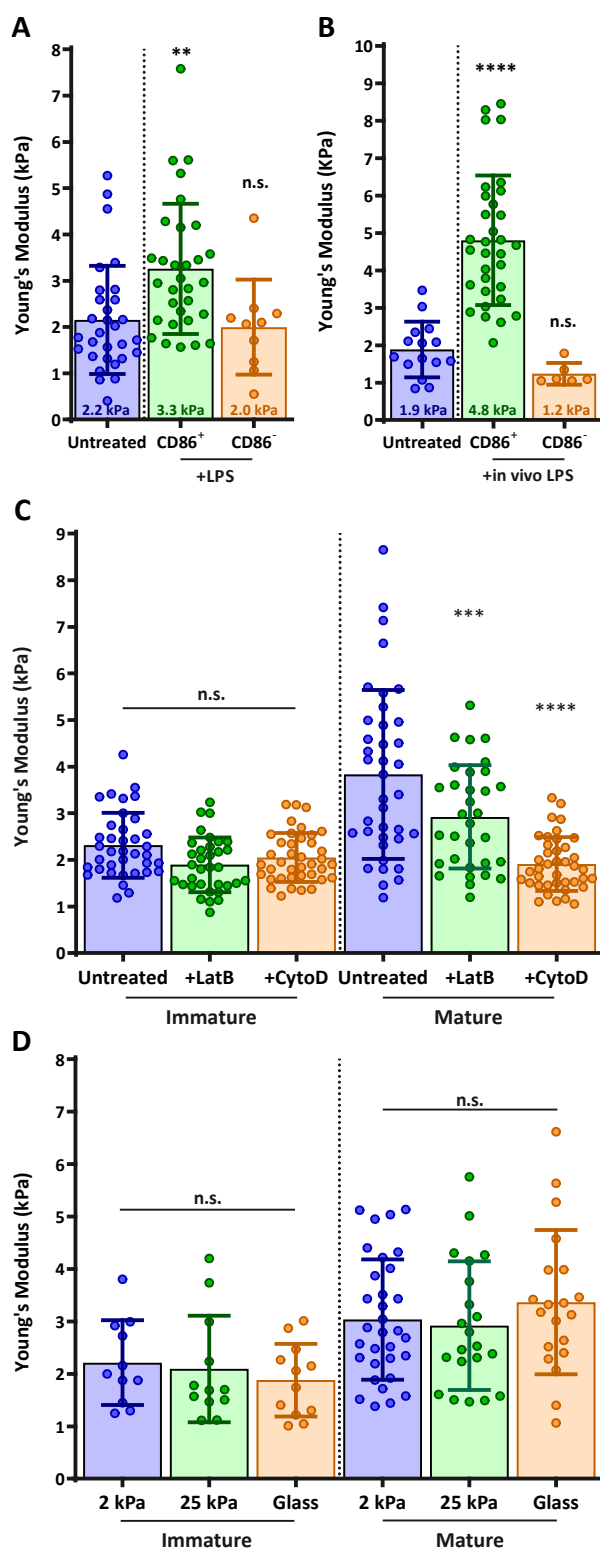


Figure 2

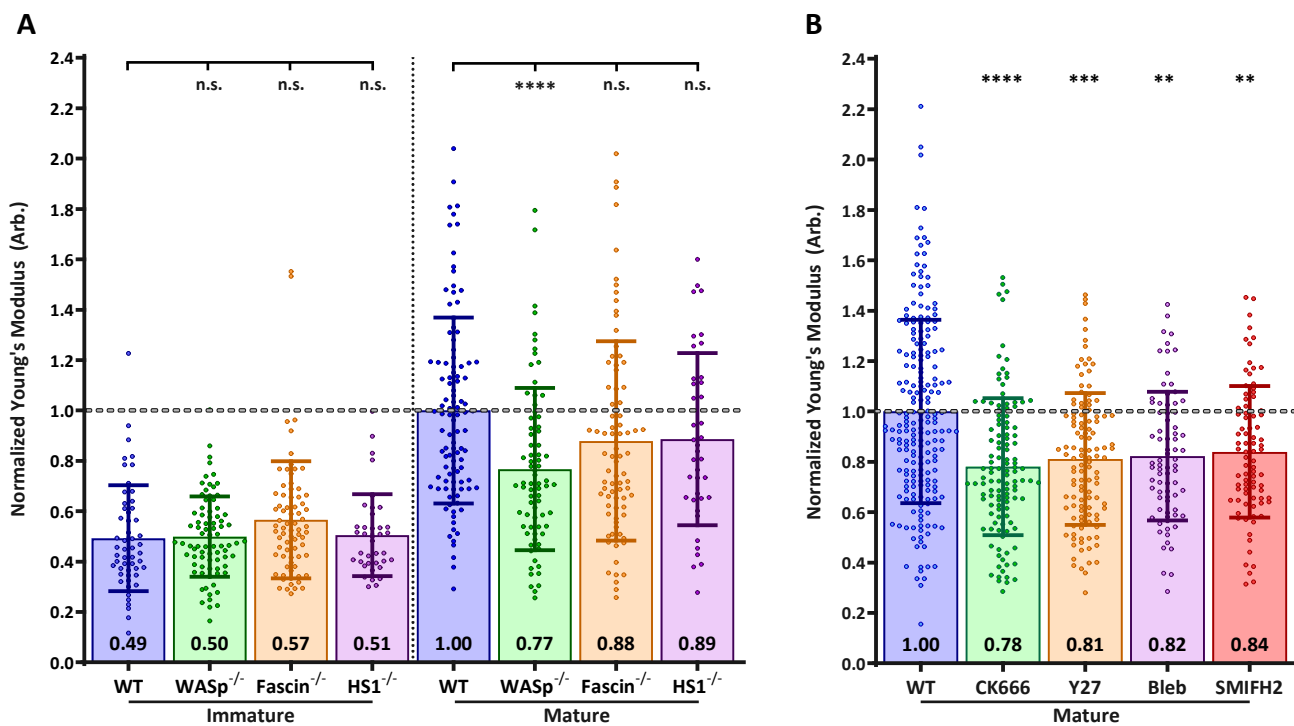


Figure 3

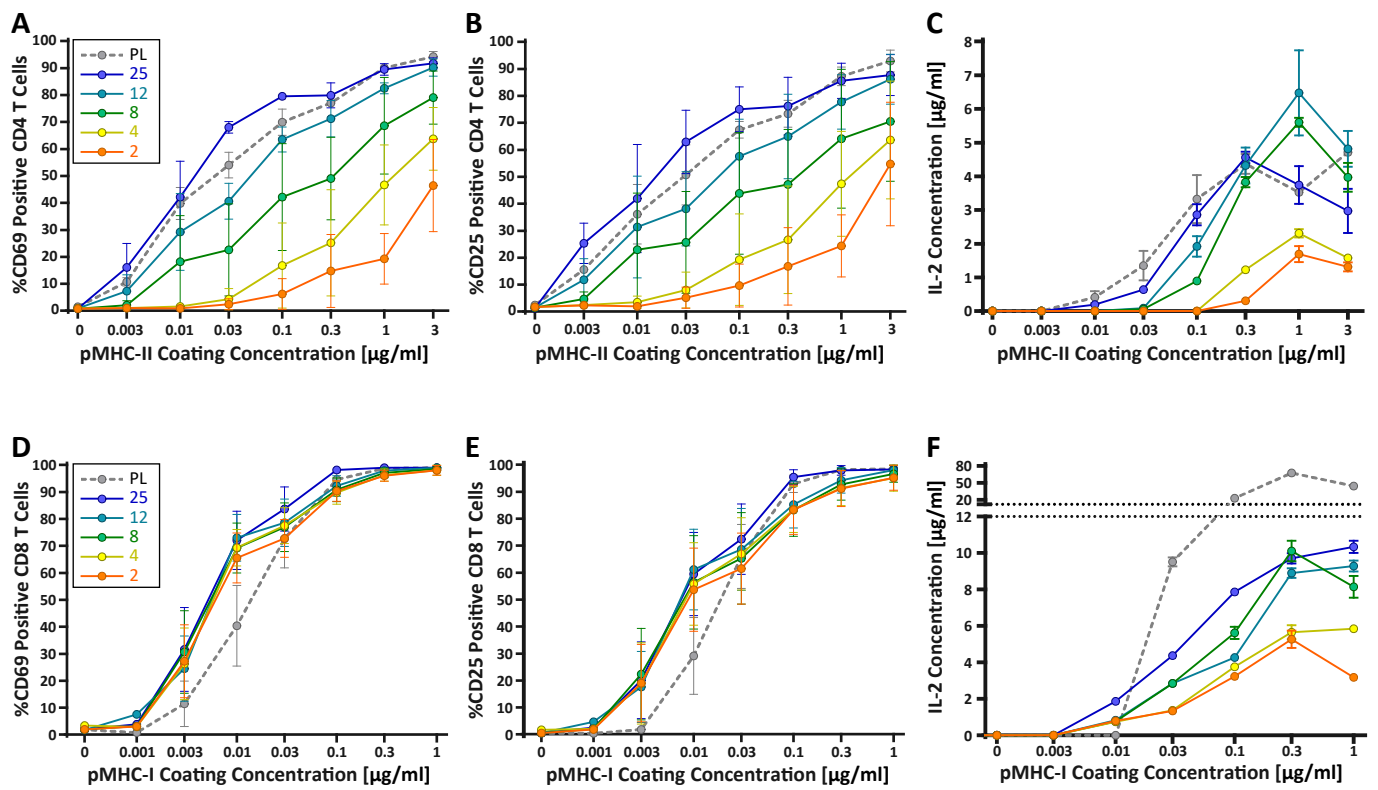


Figure 4

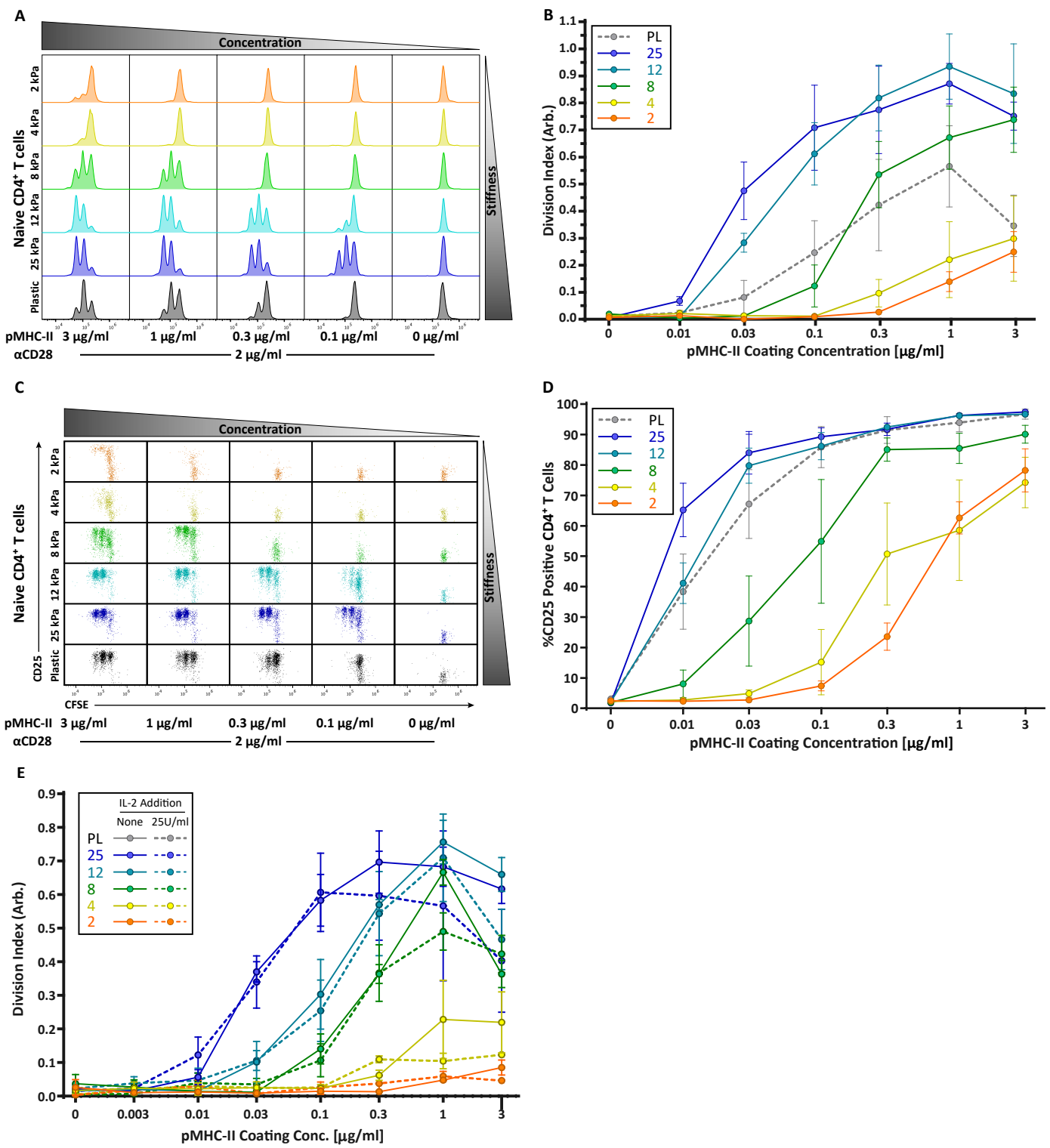


Figure 5

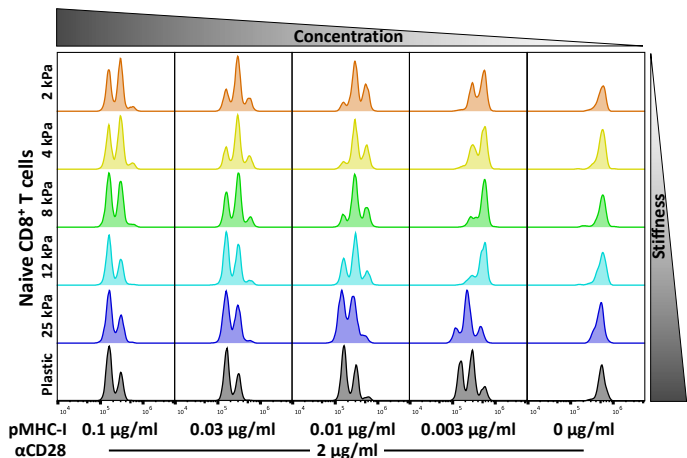
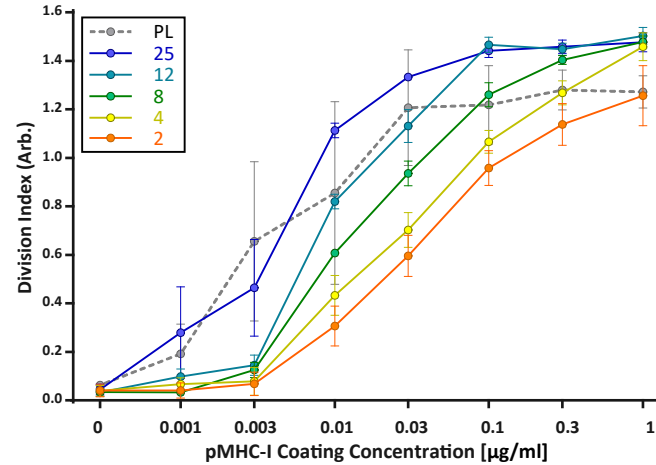
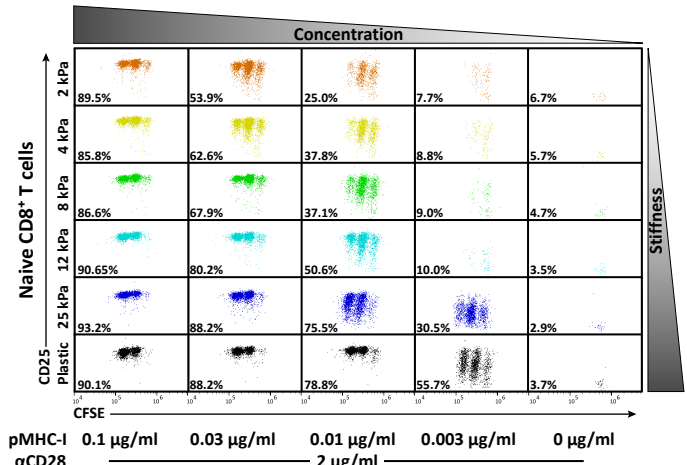
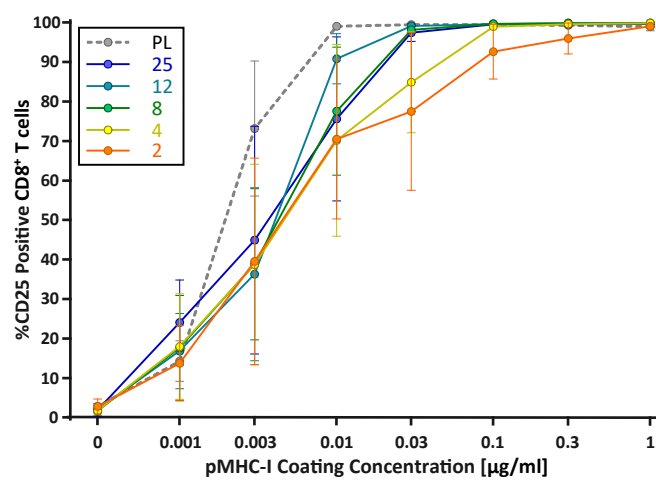
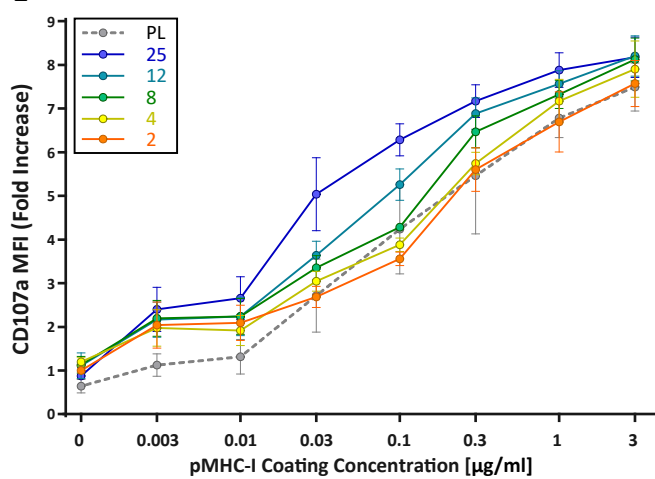
A**B****C****D****E**

Figure 6

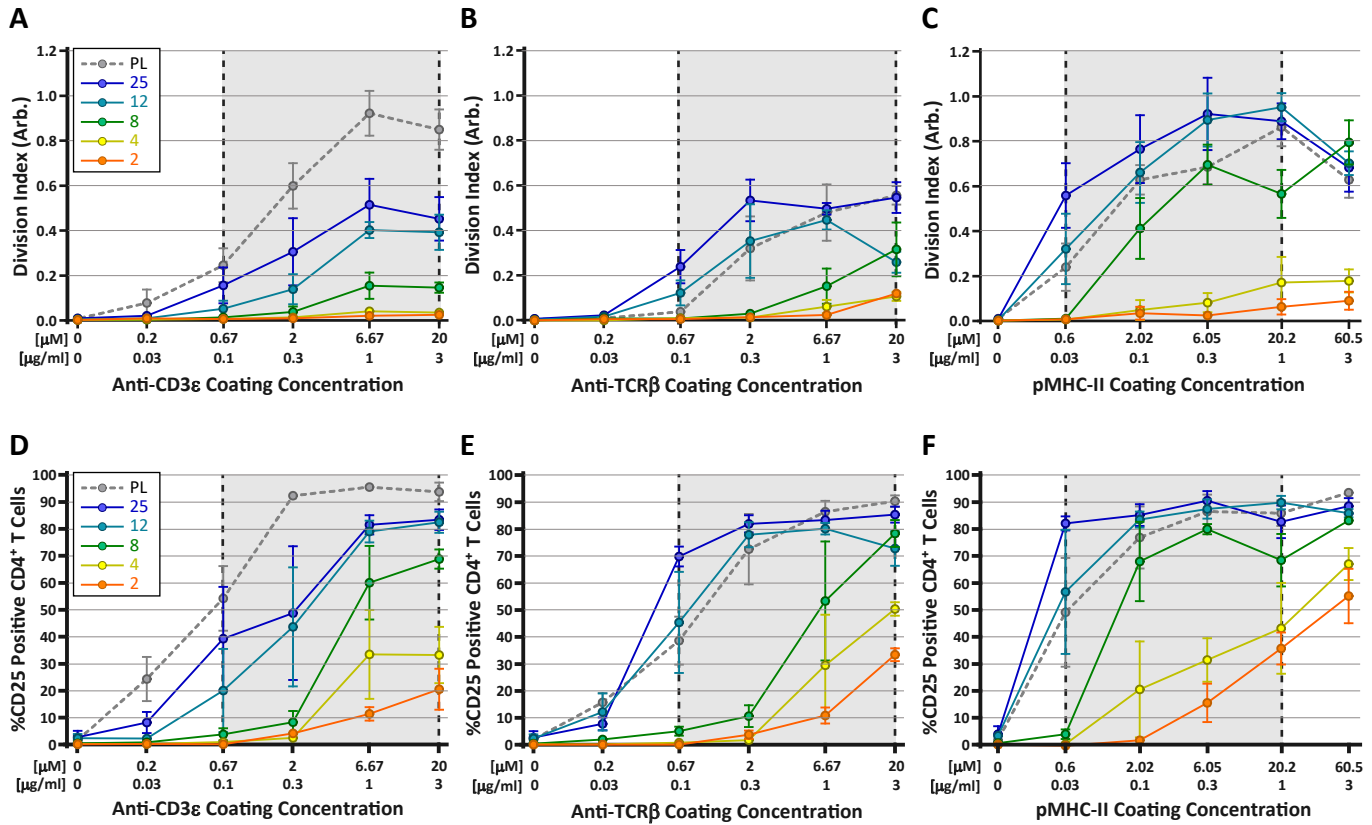


Figure 7

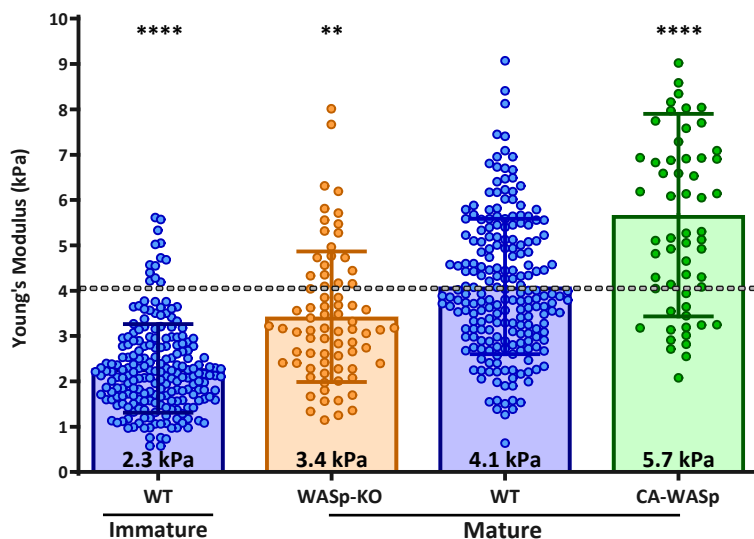
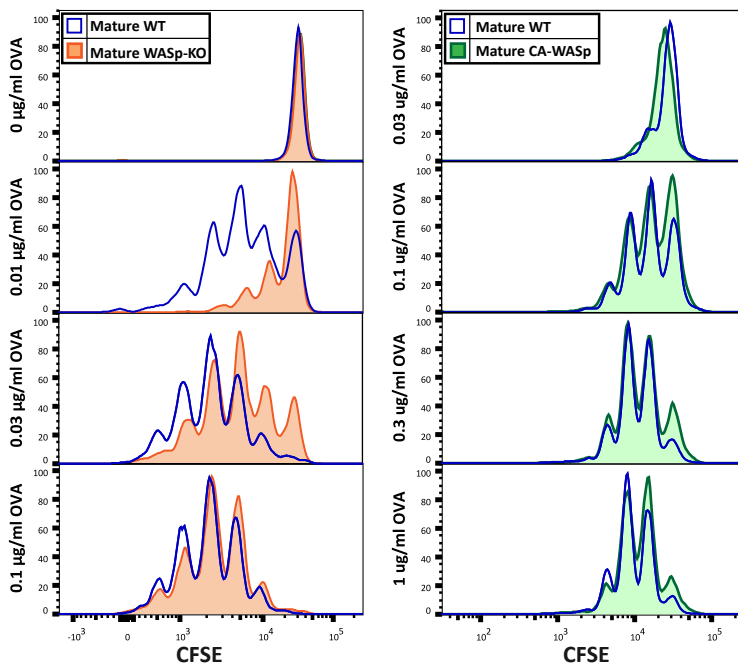
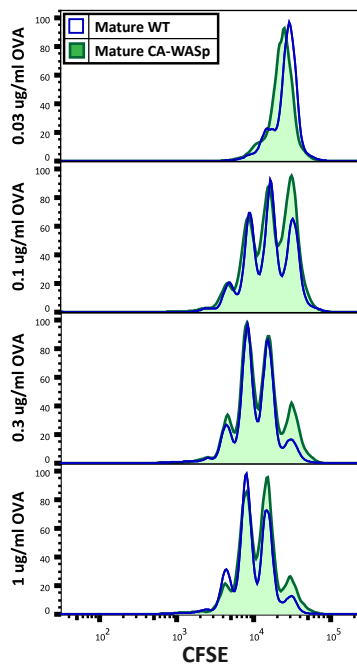
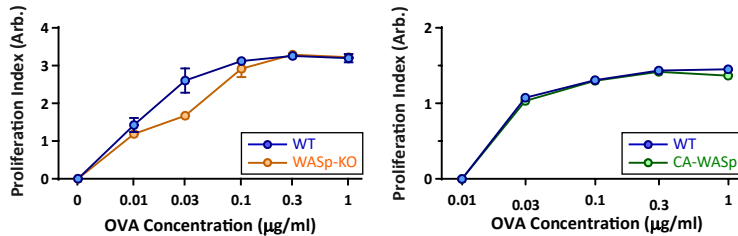
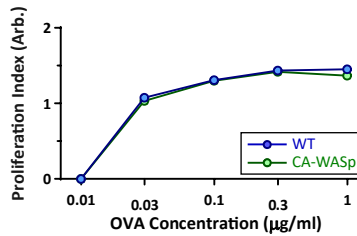
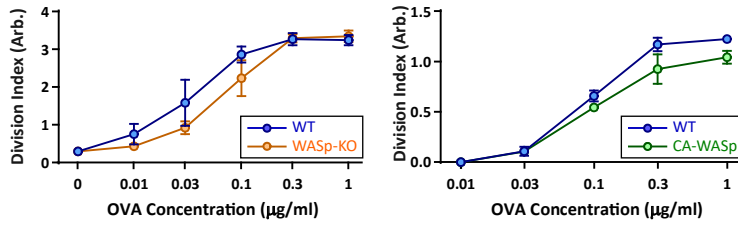
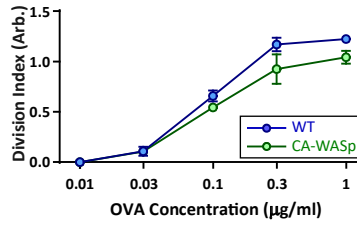
A**B****C****D****E****F****G**

Figure 1 - Figure Supplement 1

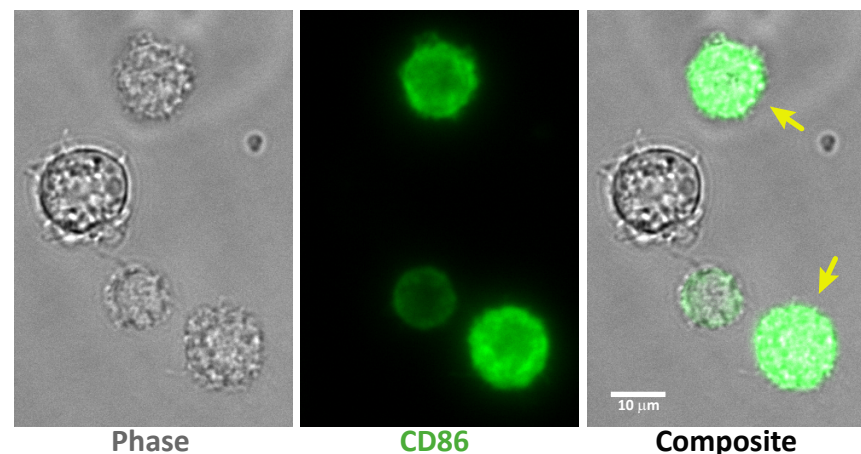


Figure 1 - Figure Supplement 2

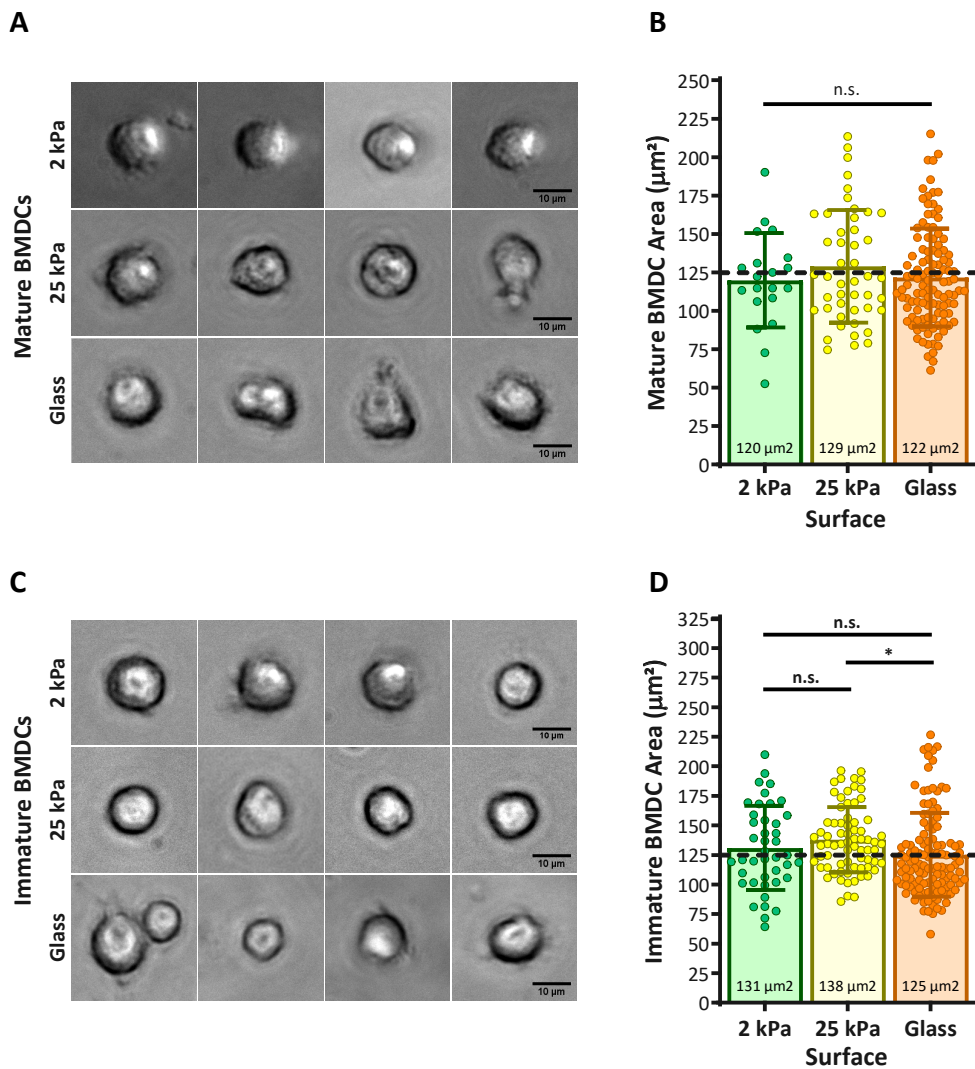
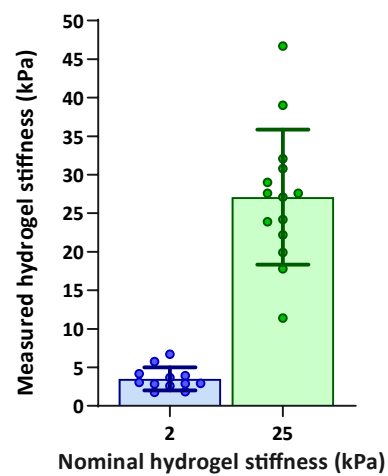


Figure 1 - Figure Supplement 3



E

Figure 1 - Figure Supplement 4

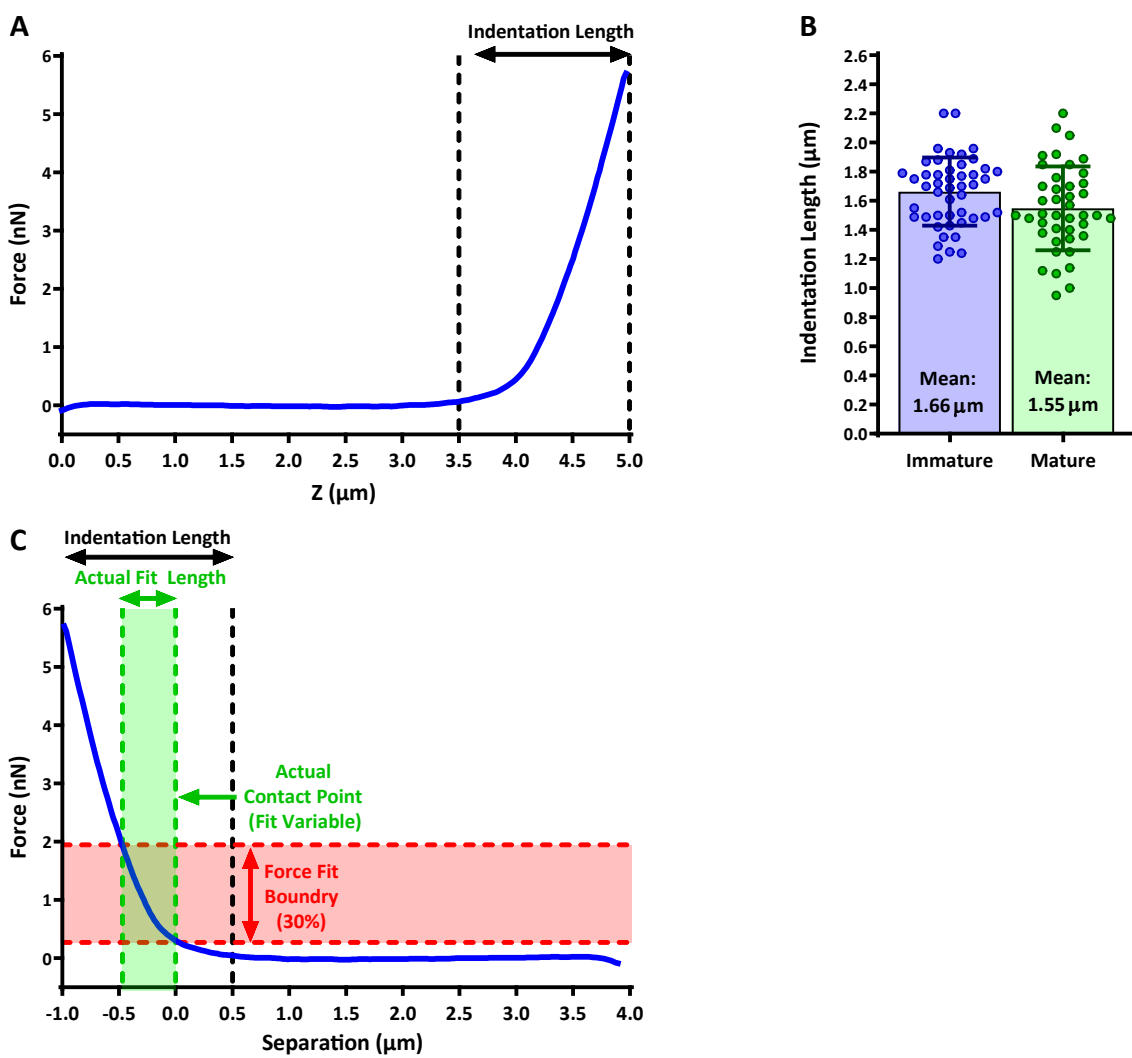


Figure 3 - Figure Supplement 1

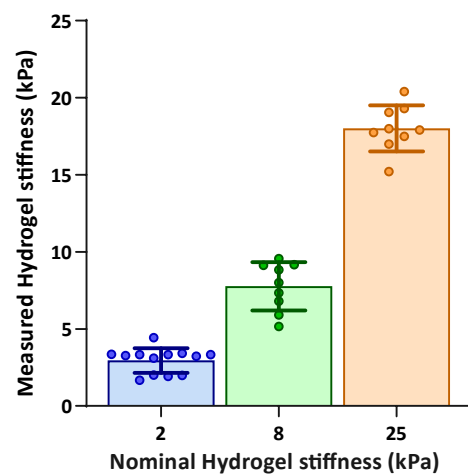


Figure 3 - Figure Supplement 2

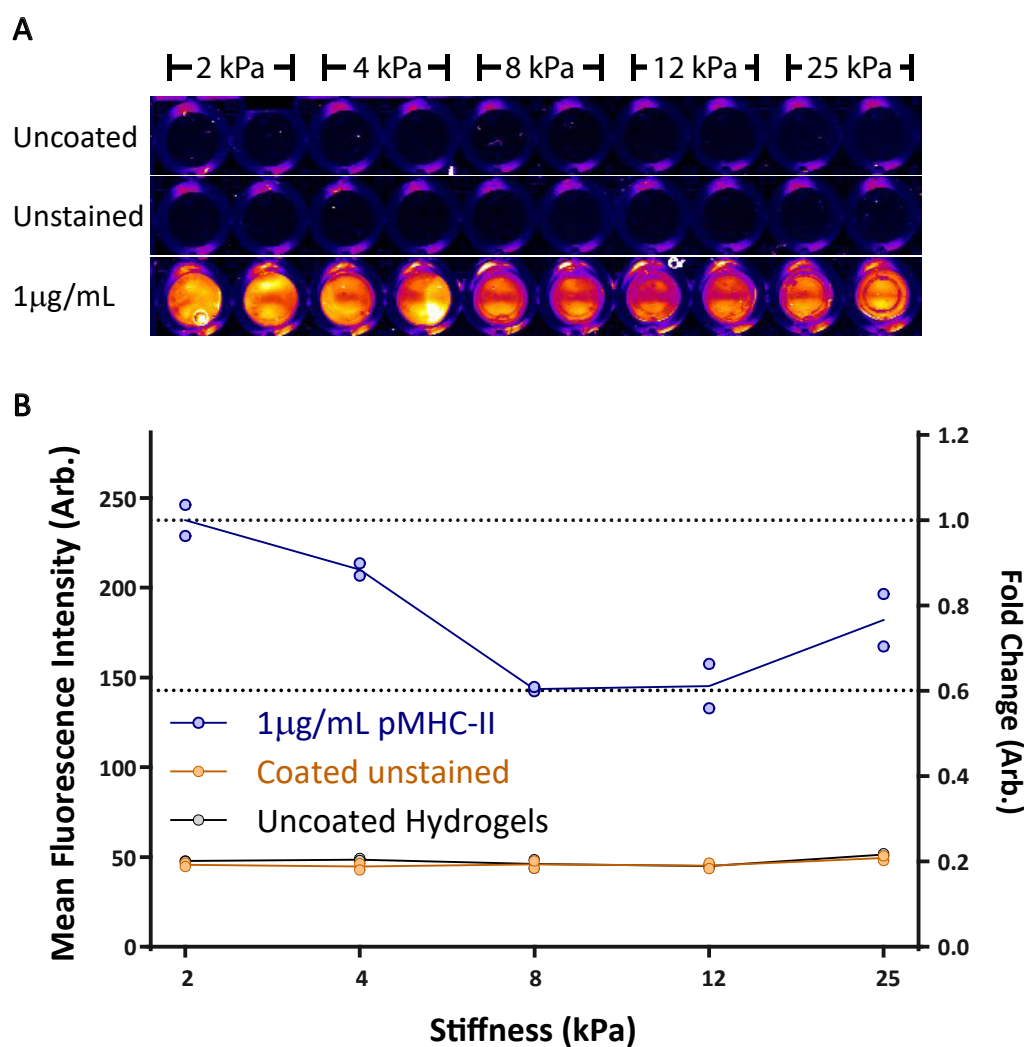


Figure 5 - Figure Supplement 1

